USGS
science for a changing world

Prepared in cooperation with the Miami-Dade County Water and Sewer Department

Three-Dimensional Seismic Characterization of Karst in the Floridan Aquifer System, Southeastern Miami-Dade County, Florida

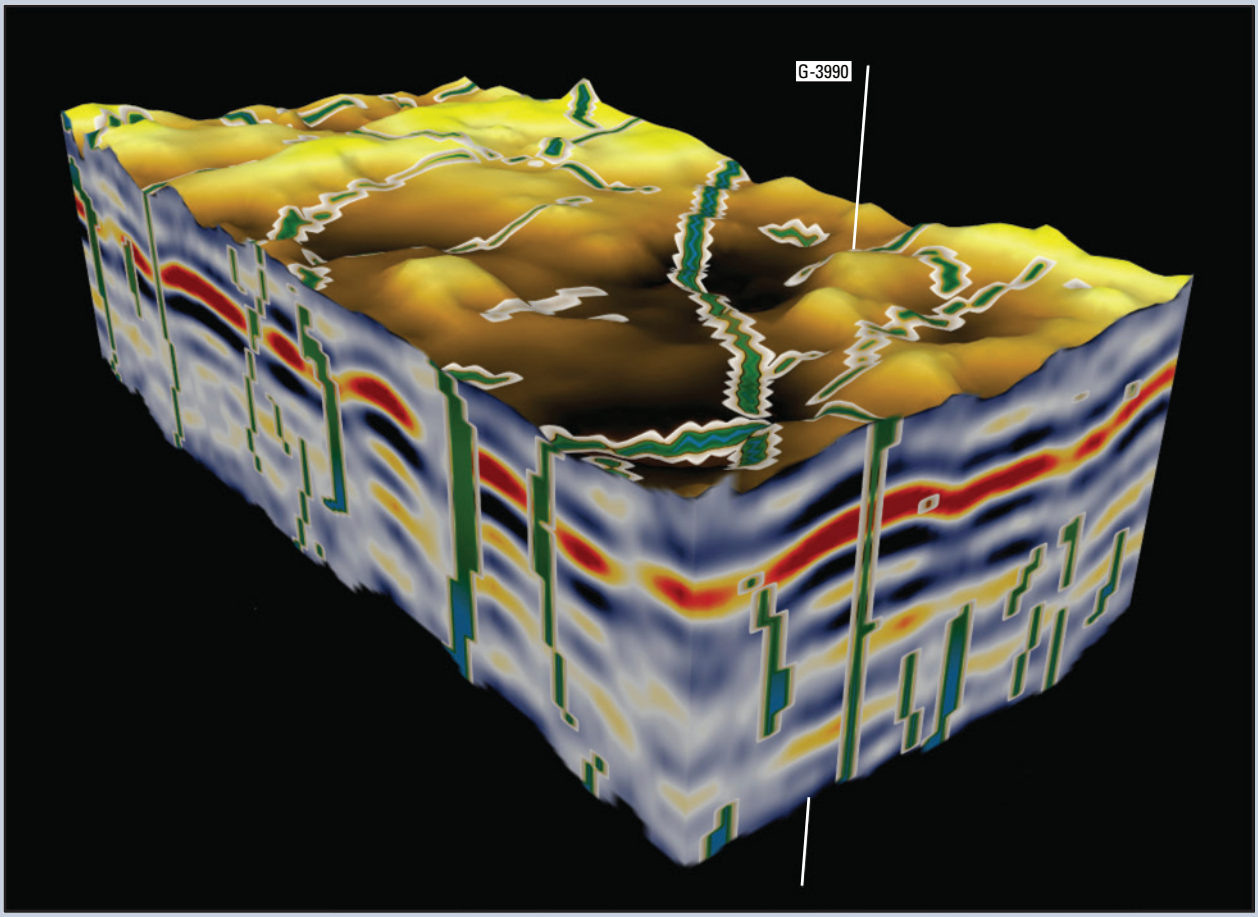

Scientific Investigations Report 2018–5117

U.S. Department of the Interior
U.S. Geological Survey

Cover. Seismic data volume of the east South Miami Heights three-dimensional seismic survey, including a time-structure map of the seismic horizon O3 as the top surface and a time-structure map of seismic horizon O1 as the base. Seismic horizons O3 and O1 are seismic sequence boundaries.

Three-Dimensional Seismic Characterization of Karst in the Floridan Aquifer System, Southeastern Miami-Dade County, Florida

By Kevin J. Cunningham, Joann F. Dixon, Richard L. Westcott, Sean Norgard, and Cameron Walker

Prepared in cooperation with the Miami-Dade County Water and Sewer Department

Scientific Investigations Report 2018–5117

U.S. Department of the Interior
U.S. Geological Survey

U.S. Department of the Interior
RYAN K. ZINKE, Secretary

U.S. Geological Survey
James F. Reilly II, Director

U.S. Geological Survey, Reston, Virginia: 2018

For more information on the USGS—the Federal source for science about the Earth, its natural and living resources, natural hazards, and the environment—visit https://www.usgs.gov or call 1–888–ASK–USGS.

For an overview of USGS information products, including maps, imagery, and publications, visit https://store.usgs.gov.

Any use of trade, firm, or product names is for descriptive purposes only and does not imply endorsement by the U.S. Government.

Although this information product, for the most part, is in the public domain, it also may contain copyrighted materials as noted in the text. Permission to reproduce copyrighted items must be secured from the copyright owner.

Suggested citation:
Cunningham, K.J., Dixon, J.F., Westcott, R.L., Norgard, S., and Walker, C., 2018, Three-dimensional seismic characterization of karst in the Floridan aquifer system, southeastern Miami-Dade County, Florida: U.S. Geological Survey Scientific Investigations Report 2018–5117, 39 p., https://doi.org/10.3133/sir20185117.

ISSN 2328-0328 (online)

Acknowledgments

The authors thank Virginia Walsh, Miami-Dade Water and Sewer Department, who granted access to the proposed South Miami Heights Water Treatment Plant. Stanley Locker, University of South Florida, and Kevin DeFosset, NOVA Southeastern University, are thanked for providing peer reviews. Daniel Ebuna, University of California—Santa Cruz, skillfully produced an application for OpendTect seismic-interpretation software that cropped seismic volumes between seismic horizons; it was used by the first author to produce seismic data volumes. Kim Swidarski, U.S. Geological Survey, assisted with illustration work.

Contents

Figures

Tables

Conversion Factors

[inch/pound to International System of Units]

Multiply	By	To obtain
	Length	
foot (ft)	0.3048	meter (m)
	Area	
square mile (mi^2)	2.590	square kilometer (km^2)
	Velocity	
foot per second (ft/s)	0.3048	meter per second (m/s)

Datum

Vertical coordinate information is referenced to the North American Vertical Datum of 1988 (NAVD 88).

Horizontal coordinate information is referenced to the North American Datum of 1983 (NAD 83).

Abbreviations

1D	one-dimensional
2D	two-dimensional
3D	three-dimensional
kHz	kilohertz
ms	millisecond
RMS	reservoir management software

Three-Dimensional Seismic Characterization of Karst in the Floridan Aquifer System, Southeastern Miami-Dade County, Florida

By Kevin J. Cunningham,[1] Joann F. Dixon,[1] Richard L. Westcott,[2] Sean Norgard,[3] and Cameron Walker[4]

Abstract

Two three-dimensional seismic surveys totaling 3.4 square miles were acquired in southeastern Miami-Dade County during 2015 as part of an ongoing broad regional investigation by the U.S. Geological Survey, in cooperation with the Miami-Dade Water and Sewer Department, that includes mapping and karst characterization of the Floridan aquifer system in southeastern Florida. Twenty columniform seismic-sag structures were identified in the three-dimensional seismic data acquired at the South Miami Heights study area in Miami-Dade County, Florida. The seismic-sag structures are commonly composed of a lower and upper seismic facies, where the lower facies is interpreted to be a high permeability column-shaped volume of intense karstification composed of faults, fractures, and collapsed caves, and the upper facies is interpreted to be a lower permeability column-shaped volume composed of sagging suprastratal reflections having little or no faulting, fracturing, or caves. The seismic-sag structures are columniform karst-collapse structures that formed by cave collapse or stoping (upward void migration caused primarily by the mechanical process of ceiling collapse) or both in carbonate rocks of the early Eocene Oldsmar Formation and in some cases in the lowermost part of the middle Eocene Avon Park Formation. Columniform subsidence and sagging of overburden succeeded karst collapse in the lower part of the structures. At the study area, there may be relatively higher potential for the columniform karst-collapse structures to provide cross-formational fluid migration upward from the Boulder Zone into the lower part of middle confining unit 2 as compared to a lower potential for cross-formational fluid migration from the upper part of middle confining unit 2 upward to the Upper Floridan aquifer.

Introduction

The disposal of treated wastewater in southern Florida (fig. 1) began in 1971 through deep-well injection of treated wastewater into a highly transmissive, saline, nonpotable zone, called the Boulder Zone, near the base of the Floridan aquifer system (fig. 2; Meyer, 1974, 1989). Since the 1990s, the treated wastewater injected into the Boulder Zone at two treated wastewater injection utilities in Miami-Dade County has been detected in an overlying brackish water interval of the upper part of the Floridan aquifer system designated as a potential alternative source of drinking water (Maliva and others, 2007; Dausman and others, 2010; Walsh and Price, 2010). This evidence for the upward movement of treated wastewater at these two Miami-Dade County wastewater disposal utilities underscores the importance of understanding the process of upward cross-formational fluid flow and identifying fluid pathways plausibly connecting the Boulder Zone to the brackish Upper Floridan aquifer of the Floridan aquifer system (fig. 2).

As part of a broad, regional hydrogeologic investigation of the Floridan aquifer system, the U.S. Geological Survey, in cooperation with Miami-Dade Water and Sewer Department, is investigating the hydrogeologic structure and characterization of karst at a proposed water-supply project to be sourced from the Biscayne aquifer (Fish and Stewart, 1991) and the Upper Floridan aquifer (fig. 2; Miller, 1986) at South Miami Heights in southeastern Miami-Dade County (fig. 1). To investigate potential for cross-formational fluid flow, two three-dimensional (3D) seismic surveys conducted over a surface area of 3.4 square miles (mi^2) were acquired in the proposed water-supply project area (fig. 1) during June–August 2015. The seismic reflection data indicate the potential for upward cross-formational flow of nonpotable

[1]U.S. Geological Survey.

[2]Cherokee Nation Businesses, contractor to the U.S. Geological Survey.

[3]Sky Valley Exploration, contractor to the U.S. Geological Survey.

[4]Walker Marine Geophysical Company, contractor to the Miami-Dade County Water and Sewer Department.

Figure 1. *A*, southern peninsular Florida and, *B*, the west and east three-dimensional (3D) seismic survey areas within South Miami Heights.

groundwater from the saline Boulder Zone upward into the Upper Floridan aquifer (fig. 2), which the U.S. Environmental Protection Agency (2013) designated an underground source of drinking water.

This report provides a preliminary interpretation of the three-dimensional (3D) seismic data to improve existing knowledge about the spatial distribution of vertical cross-formational fluid-flow pathways in the Floridan aquifer system that are likely present within the South Miami Heights study area (fig. 1). Maps of four seismic horizons, seismic data volumes, and seismic profiles are presented that provide information essential to subsurface hazard assessment, regional water-resource management, and planning for construction of the proposed South Miami Heights water treatment plant. Research on the hydrogeology, sequence stratigraphy, structure, and buried karst features of the carbonate rocks composing much of the Floridan aquifer system (fig. 2) in southeastern Florida is supported by this presentation of seismic data. A statistical approach to neural network imaging of karst systems that used the South Miami Heights 3D seismic data (Ebuna and others, 2018) provides further characterization of the karst system within the carbonate rocks of the Floridan aquifer system in the study area.

Methods

Twelve seismic horizon structural altitude maps, eight 3D seismic data volumes, and four interpreted seismic profiles were produced for this study using several types of data. The data types include (1) 3D, high-resolution, multichannel, seismic data; (2) geophysical log data from 5 test wells and 1 test corehole (G-3979, G-3982, G-3983, G-3984, G-3986, and G-3990; table 1, fig. 1); (3) 7 feet (ft) of optical borehole-wall image data from the G-3990 test well (table 2); and (4) a single synthetic seismogram constructed using sonic log data acquired from the G-3990 test well (table 1; figs. 1, 2).

Seismic Data Acquisition, Processing, and Interpretation

During June–August 2015, Walker Marine Geophysical Company acquired high-resolution, multichannel, 3D seismic-reflection data over a 3.4-mi^2 area using a single mobile Inova Univib seismic vibrator (fig. 3) and Geospace GCX1 autonomous nodal receivers (fig. 4) to produce two 3D seismic surveys in a densely populated suburban area of southeastern Miami-Dade County (fig. 1). The seismic data are owned by Miami-Dade Water and Sewer Department. The vibroseis method used to acquire these seismic data is well documented (for example, Chapman and others, 1981; Baeten, 1989). One seismic survey acquisition area, designated the west South Miami Heights seismic survey, covers 0.99 mi^2 (fig. 5) and the second survey acquisition area, designated the east South Miami Heights seismic survey, covers a 2.41-mi^2 area (fig. 6). The west South Miami Heights seismic survey contained 318 active nodal receivers and 602 acoustic source locations (fig. 5), also known as vibrator points. The east South Miami Heights seismic survey contained 697 active nodal receivers and 1,629 vibrator points (fig. 6). During seismic data processing, each of the two seismic surveys were divided into rows and columns of square bins that served as electronic containers for digital information, analogous to pixels in the image sensor of a digital camera. The dimensions of each bin measured 82.5 by 82.5 ft and were selected as one-half the distance of the 165-ft nodal receiver spacing. In the processing of seismic traces, the total number of bins produced 52 east-west oriented inline and 52 north-south oriented crossline seismic profiles for the west South Miami Heights seismic survey (figs. 1, 5), and 59 inlines and 108 crosslines for the east South Miami Heights seismic survey (figs. 1, 6). The Inova Univib vibrator was configured at 26,000 peak pound-force, but was operated at 60 to 70 percent of that force. Seismic data were acquired at a 4-kilohertz (kHz) sample rate.

Walker Marine Geophysical Company provided quality-control and quality-assurance of the seismic data and delivered the data to Excel Geophysical Services for final processing, stacking, and migration. The processed zero-time datums of both seismic surveys is relative to the North American Vertical Datum of 1988 (NAVD 88). The generalized processing steps applied to the acquired data included resampling data to 2 kHz at 0.5-millisecond (ms) intervals, auto-gain control, velocity analysis, normal move out, muting, datum statics, residual and trim statics, common mid-point stacking, deconvolution, and time migration. The data acquired at 4 kHz were resampled at 2 kHz to reduce processing cost; the processing was sensitive to assuring that the reduction in sampling did not also cause a decrease in data quality. For data having substantial high-frequency noise, however, a lower band-pass frequency was used to reduce the high-frequency noise and improve the signal-to-noise ratio. Figure 7 shows a typical frequency versus amplitude spectrum for the seismic surveys.

The interpretation of seismic data for this study mainly involved the identification and characterization of seismic-reflection termination, configuration, continuity, and amplitude produced by sedimentary strata (Mitchum and others, 1977), and of seismic attributes generated by seismic interpretation software. The seismic stratigraphy developed for the Eocene to Pleistocene strata of Broward County by Cunningham and others (2018) was used as the fundamental seismic-sequence framework for the study area.

Synthetic Seismogram

A synthetic seismogram is a one-dimensional (1D) model of acoustic energy traveling through the stratum of the Earth and is displayed as a waveform (fig. 2). A single synthetic seismogram was produced from borehole-compensated

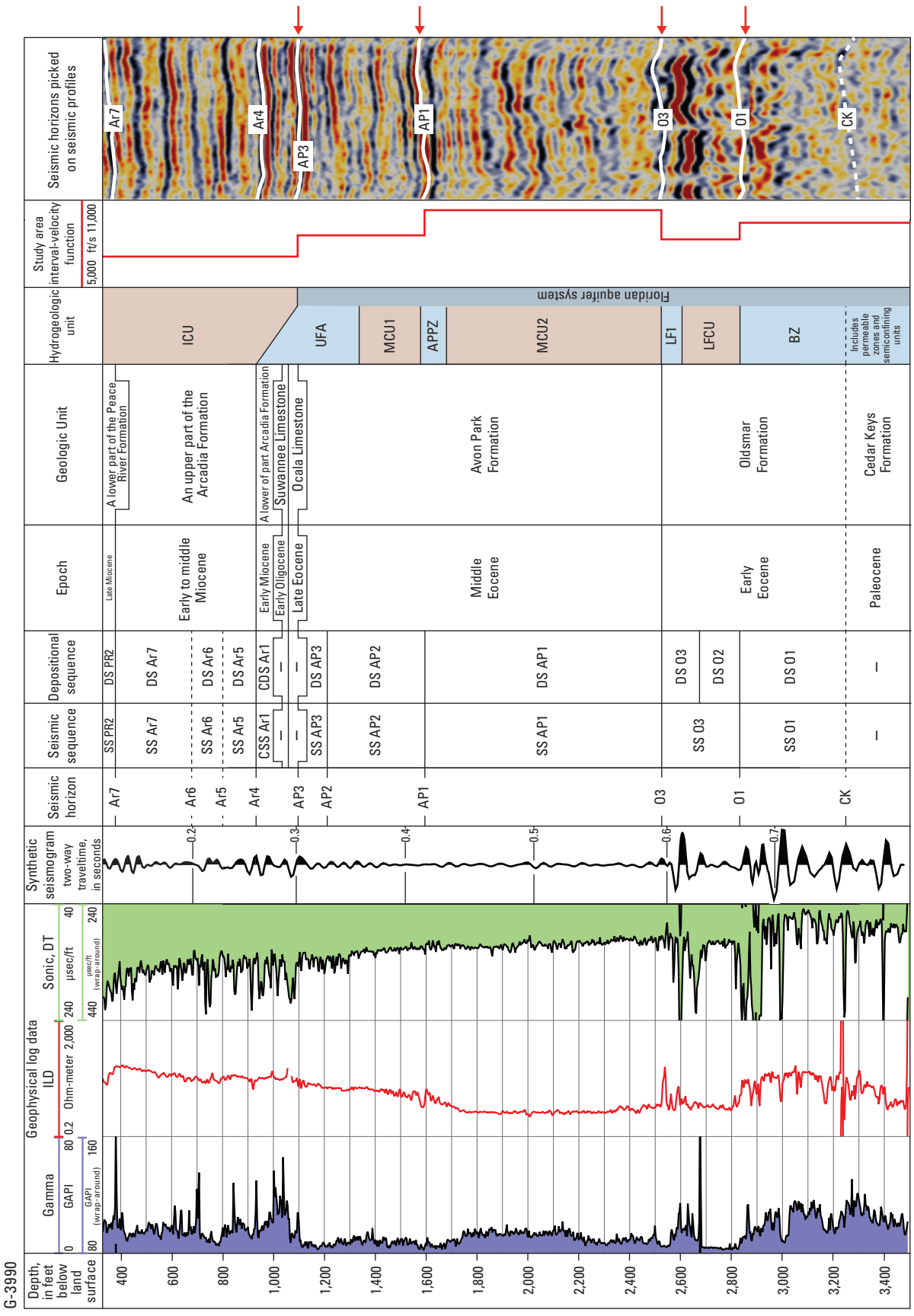
G-3990
Depth, in feet below land surface
Geophysical log data
Gamma
0 GAPI 80
80 GAPI (wrap-around) 160
ILD
0.2 Ohm-meter 2,000
Sonic, DT
240 µsec/ft 40
440 µsec/ft (wrap-around) 240
Synthetic seismogram two-way traveltime, in seconds
Seismic horizon
Seismic sequence
Depositional sequence
Epoch
Geologic Unit
Hydrogeologic unit
Study area interval-velocity function
5,000 ft/s 11,000
Seismic horizons picked on seismic profiles
Ar7
Ar4
AP3
AP1
O3
O1
CK
Florida aquifer system
ICU
UFA
MCU1
APPZ
MCU2
LF1
LFCU
BZ
Includes permeable zones and semiconfining units
A lower part of the Peace River Formation
An upper part of the Arcadia Formation
A lower of part Arcadia Formation
Suwannee Limestone
Ocala Limestone
Avon Park Formation
Oldsmar Formation
Cedar Keys Formation
Late Miocene
Early to middle Miocene
Early Miocene
Early Oligocene
Late Eocene
Middle Eocene
Early Eocene
Paleocene
DS PR2
DS Ar7
DS Ar6
DS Ar5
CDS Ar1
DS AP3
DS AP2
DS AP1
DS O3
DS O2
DS O1
SS PR2
SS Ar7
SS Ar6
SS Ar5
CSS Ar1
SS AP3
SS AP2
SS AP1
SS O3
SS O1
Ar6
Ar5
AP2
0.2
0.3
0.4
0.5
0.6
0.7
400
600
800
1,000
1,200
1,400
1,600
1,800
2,000
2,200
2,400
2,600
2,800
3,000
3,200
3,400

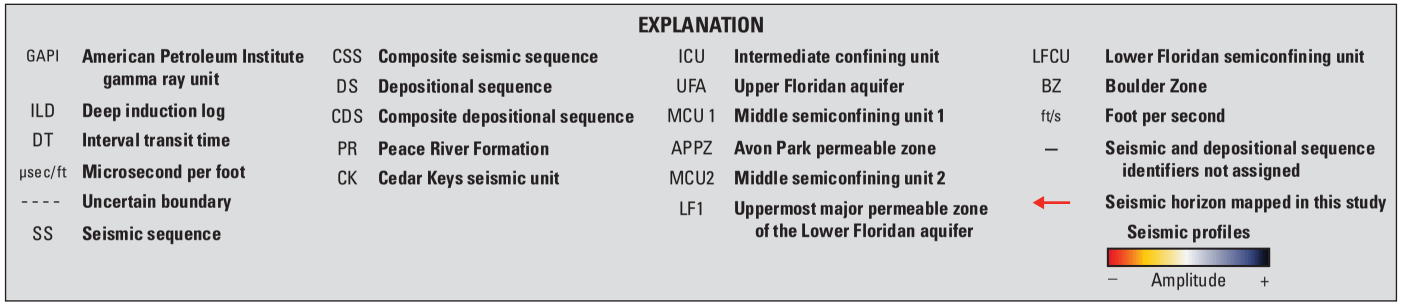

Figure 2. Relations between geophysical log data from the G-3990 test well, seismic survey data from the study area, and the local hydrogeologic framework. The seismic data on the right side of the chart have been stretched or compressed to match the depth scale in feet on the left side of the chart. Geophysical log data were obtained from the Miami-Dade Water and Sewer Department.

Table 1. Identifiers, locations, and other information for all wells used in the study.

[Geophysical log data acquired from the six wells listed are owned by Miami-Dade County and are not archived in a data release. Horizontal coordinates referenced to North American Datum of 1983. USGS, U.S. Geological Survey]

USGS well identifier	Other well identifier	USGS site identification number	State Plane Easting (feet)	State Plane Northing (feet)	Total depth (feet below land surface)	Used in producing synthetic seismograms	Used for lithostratigraphy and cyclostratigraphy from core
G-3979	C-1	261538080092801	860369.70	451120.49	1,650	No	Yes
G-3982	TPW-3	261445080154801	860084.14	451105.12	1,404	No	No
G-3983	TPW-2	261445080154801	855199.67	451339.98	1,400	No	No
G-3984	TPW-1	261548080060201	860263.04	454157.88	1,401	No	No
G-3986	DZMW-1	260540080075001	861141.27	450403.34	1,708	No	No
G-3990	IW-1B	260543080075601	861193.39	450405.89	3,500	Yes	No

Table 2. Information for optical borehole-wall image data acquired at test well G-3990.

[Location and other information for test well are shown in figure 1 and table 1. Dates shown as month, day, year. NWIS, National Water Information System. USGS, U.S. Geological Survey]

Collection information				Measured values				Logging tool information					
NWIS site number	Log date	Log category	Logging unit agency	Depth start (feet)	Depth end (feet)	Log measuring point height (feet)	Log measuring point reference	Serial number	Manufacturer	Model	Calibration date and time	Calibration description	Remarks
253417080224102	1/31/17	Optical televiewer	USGS	1,705	1,709	0.00	Land surface	151101	ALT-Advanced Logic Technology	QL40-OBI-2G	4/28/2015 12:00 a.m.	Factory	Image collected at 900 turn rate and 0.0041 sample rate.
253417080224102	1/31/17	Optical televiewer	USGS	2,869	2,872	0.00	Land surface	151101	ALT-Advanced Logic Technology	QL40-OBI-2G	4/28/2015 12:00 a.m.	Factory	Image collected at 900 turn rate and 0.0041 sample rate.

Figure 3. Inova Univib vibrator used in acquisition of the three-dimensional (3D) seismic surveys for this study.

Figure 4. Geospace GCX1 autonomous nodal receivers used for the acquisition of the three-dimensional (3D) seismic surveys for this study.

sonic log data acquired by the Miami-Dade Water and Sewer Department at the deepest test well (G-3990) in the study area (fig. 1). The sonic log data were converted to a synthetic seismic wavelet and a time-depth curve using the synthetic-seismogram production module SynPAK in the IHS Kingdom seismic and geological interpretation software. The synthetic seismic wavelet was used to directly match specific seismic horizons on seismic profiles to key subsurface stratigraphic markers identified in the 1D geophysical log data acquired from the G-3990 test well (fig. 2).

Interval-Velocity Function

The study area interval-velocity function comprises five interval velocities (that is, average seismic velocities calculated for each depth-interval thickness) at the G-3990 test well (fig. 2). From bottom to top, the five interval velocities were calculated between the following: the total depth of the G-3990 test well and seismic horizon O1, seismic horizons O1 and O3, seismic horizons O3 and AP1, seismic

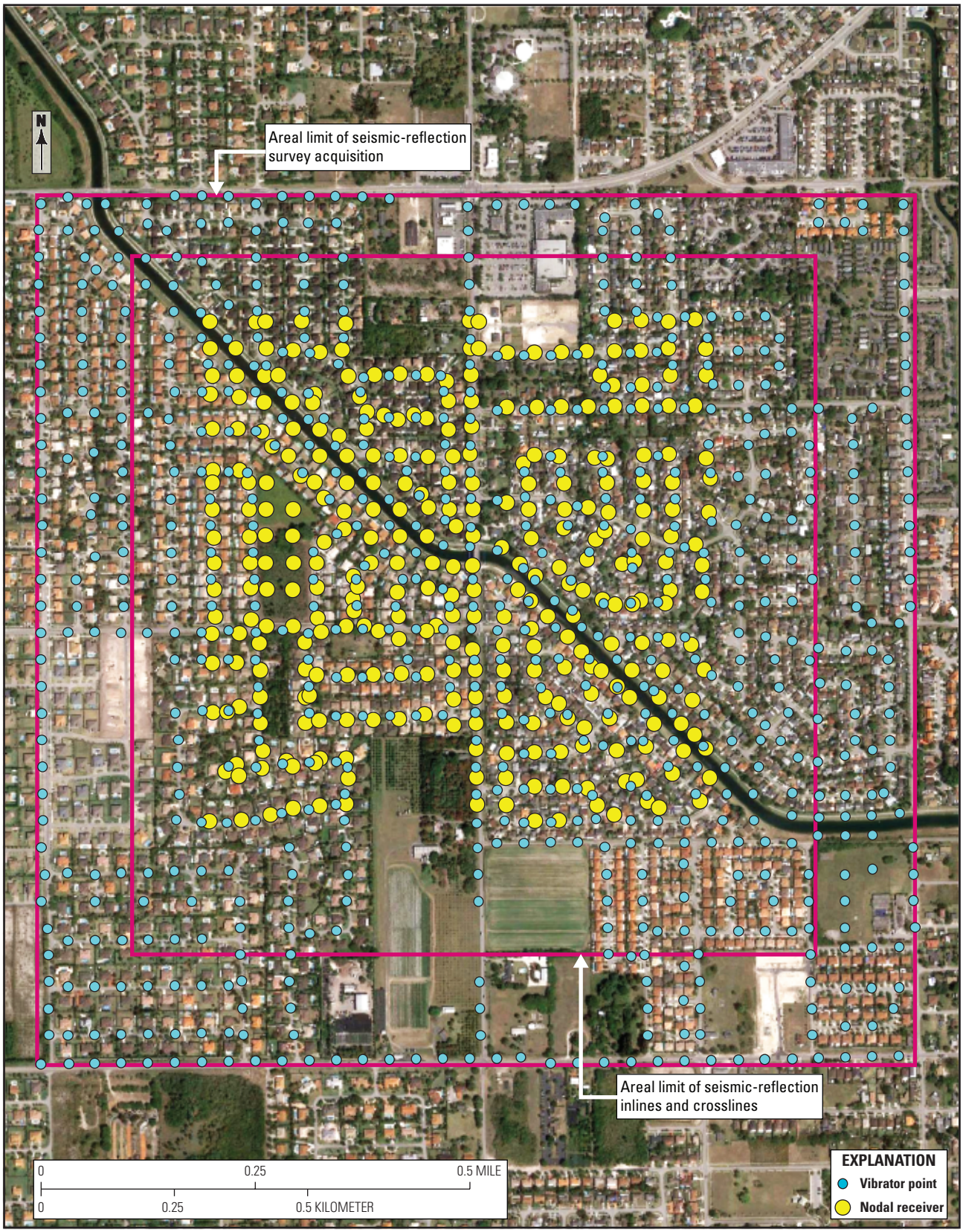

Base map data from Google, 2017

Figure 5. Configuration of vibrator points and autonomous nodal receivers at the west South Miami Heights three-dimensional (3D) seismic survey areas (fig. 1). The aerial imagery was used to show the dense suburban environment where the seismic reflection survey was completed.

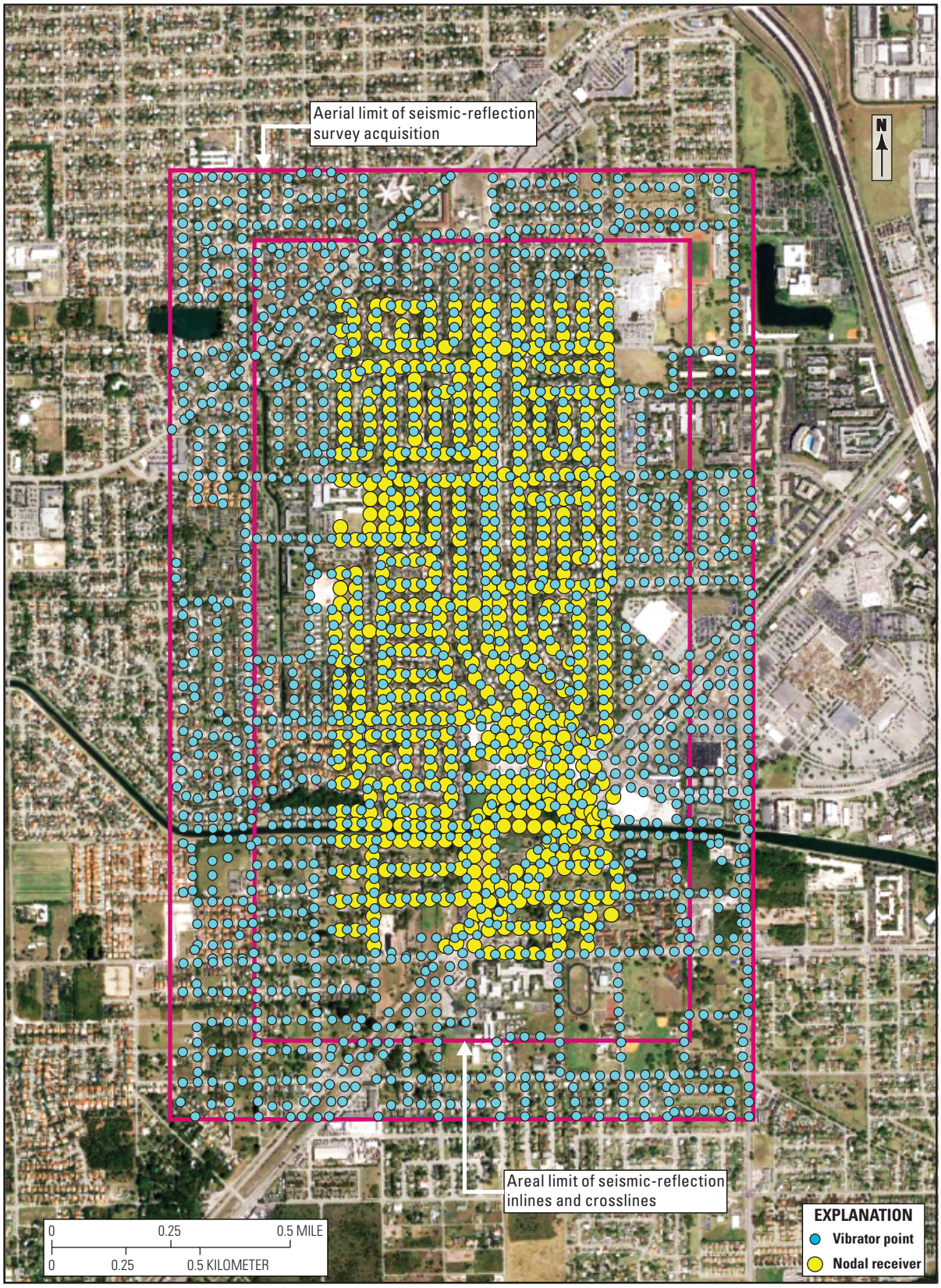

Base map data from Google, 2017

Figure 6. Configuration of vibrator points and autonomous nodal seismic receivers at the east South Miami Heights three-dimensional (3D) seismic survey areas (fig. 1). The aerial imagery was used to show the dense suburban environment where the seismic reflection survey was completed.

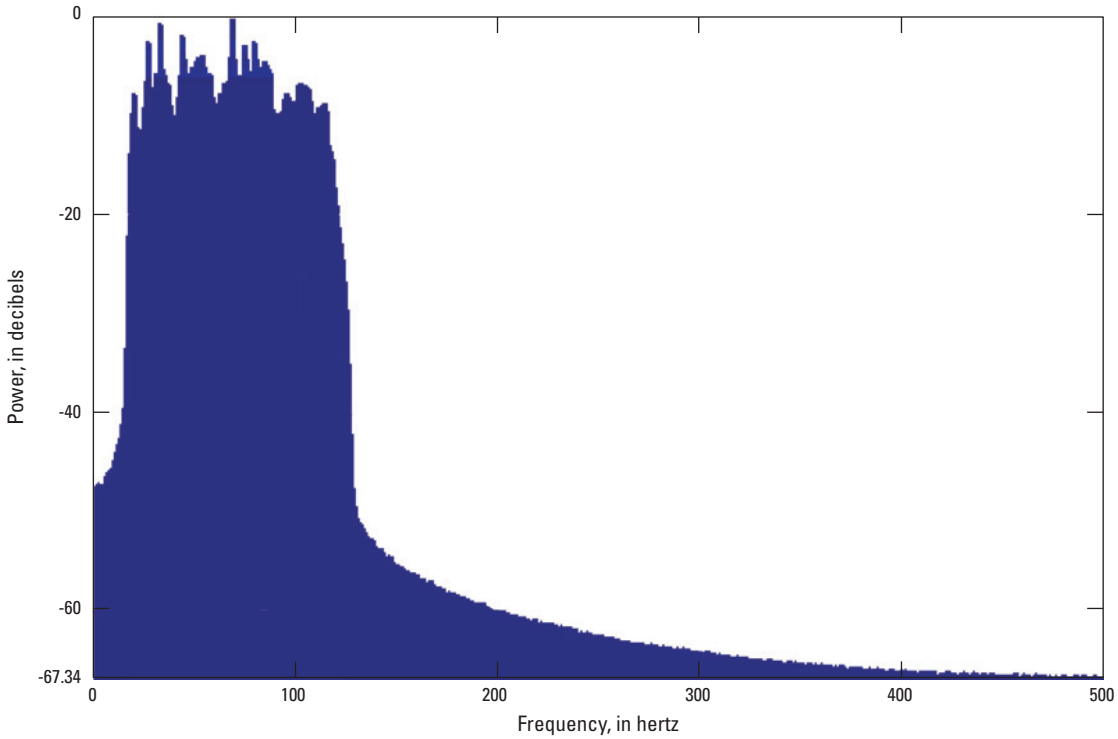

Figure 7. Typical frequency versus amplitude histogram spectrum for seismic data acquired in the study area (fig. 1). Data were extracted from inline 32 of the east South Miami Heights seismic survey.

horizons AP1 and AP3, and seismic horizon AP3 and the seismic datum (NAVD 88). In the study area, only the G-3990 test well penetrates the upper boundaries of depositional sequences O1 and O2 (equivalents to seismic horizons O1 and O2, respectively); therefore, the other four test wells and test corehole (fig. 1, table 1) were not used for developing the single interval-velocity function for the study area (fig. 2). The calculated interval velocities for each of the five depth intervals used in the G-3990 test well are shown in table 3.

Table 3. Calculated interval velocities at the G-3990 test well.

[Test well location shown in figure 1. NAVD 88, North American Vertical Datum of 1988]

Interval	Interval velocity (one-way travel time, in feet per second)
Seismic horizon AP3 to seismic datum at NAVD 88	7,146
Seismic horizon AP1 to AP3	8,690
Seismic horizon O3 to AP1	10,438
Seismic horizon O1 to O3	8,444
Total depth of G-3990 test well to seismic horizon O1	9,580

Horizon Maps, Seismic-Data Volumes, and Fault Mapping

In creating the horizon maps for the South Miami Heights study area, the first task was to identify the four major seismic horizons of the Oldsmar and Avon Park Formations mapped by Cunningham and others (2018) in a Broward County seismic study with the exception of seismic horizon AP2 (fig. 2). Two steps were used to identify the four seismic horizons—O1, O3, AP1, and AP3 (fig. 2)—in the study area. First, the seismic stratigraphy of Cunningham and others (2018) was correlated with the seismic stratigraphy at the west and east South Miami Heights 3D seismic surveys. Second, the reflection patterns produced from the seismic surveys were matched to geophysical log data and the synthetic seismogram from the G-3990 test well (fig. 2). Each of the four seismic horizons corresponds, or nearly corresponds, to the key seismic sequence boundaries and depositional sequence boundaries O1, O3, AP1, and AP3 (fig. 2). The open-source OpendTect seismic interpretation software was used for "picking" (a process of interpreting and gathering seismic horizon data) from the four seismic horizons (O1, O3, AP1, and AP3, fig. 2) to construct four time-structure maps for both the west and east South Miami Heights seismic surveys; consequently, a total of eight time-structure maps were produced. These maps, displayed in acoustic two-way traveltime, were used as the upper bounding surface on eight seismic volumes generated in OpendTect for the west and east South Miami Heights 3D seismic surveys (fig. 1). In addition, the eight time-structure maps were next

imported into the ROXAR (Emerson, St. Louis, Missouri) reservoir management software (RMS). ROXAR RMS was utilized to convert the time-structure maps to structural altitude maps relative to the NAVD 88 datum and using the calculated interval velocities, expressed in feet per second, at the G-3990 test well (table 3). Three visualization formats were used to display 12 ROXAR-RMS-produced structural altitude maps created for the west and east South Miami Heights seismic surveys. The three visualization formats are (1) a two-dimensional (2D) structural altitude map, (2) a 2D structural altitude map with a transparent Google Map overlay, and (3) a 3D structural altitude map. Lastly, each of the eight time-structure maps were simply used as the upper bounding surface on eight seismic volumes generated in OpendTect for the west and east South Miami Heights 3D seismic surveys.

The mapping of highly probable locations for faults was achieved using the OpendTect Faults & Fractures plugin. This plugin is an image processing algorithm used to produce a thinned-fault-likelihood attribute that is displayed as a fault-trace image on the mapped seismic horizon surfaces and vertical seismic profiles within the OpendTect software environment. For this study, as a final step in the production of structural altitude maps, traces of the thinned-fault-likelihood attribute were projected and traced as faults onto eight of the 2D structural altitude maps within the Adobe Illustrator CC graphical software environment. The tracing of the faults onto the eight structural altitude maps was only done for the two types of maps, the two-dimensional (2D) structural altitude maps and the 2D structural altitude maps with a transparent Google Map overlay. Furthermore, the thinned-fault-likelihood attribute was displayed on the eight seismic volumes within the OpendTect software environment.

Preliminary Seismic Characterization of Karst

Twelve structural altitude maps, eight seismic data volumes, and four seismic profiles are presented in this preliminary seismic characterization of karst in the Floridan aquifer system of the study area. The maps, data volumes, and profiles provide visualizations that were used to characterize the karst with an emphasis on columniform seismic-sag structures (compare to "circular sag structures" of McDonnell and others, 2007, p. 1296) and bead-string reflections (Rao and Wang, 2015).

Numerous vertical and semivertical columniform seismic-sag structures have been identified on seismic profiles from many carbonate provinces worldwide (Popenoe and others, 1984; Hardage and others, 1996; Kindinger and others, 1999; Spechler, 2001; Heubeck and others, 2004; McDonnell and others, 2007; Cunningham and Walker, 2009; Hine and others, 2009; Betzler and others, 2011; Sun and others, 2013; Barnett and others, 2015; Cunningham, 2015; Burberry and others, 2016; Cunningham and others, 2018). These seismic structures imaged within carbonate platforms have also been called chimneys (Betzler and others, 2011) and pipes (Sun and others, 2013; Chen and others, 2015). In southeastern Florida, Cunningham and Walker (2009) first described the presence of buried, vertical, columniform seismic-sag structures on seismic profiles acquired in Biscayne Bay. The physical manifestation of the seismic-sag structures as columniform karst-collapse structures could have an impact on potential cross-formational fluid flow within the carbonate rocks of the Floridan aquifer system (fig. 2). Small, anomalous bead-string reflections on seismic profiles of the Tarim Basin in northwestern China have been reported as evidence for seismic-scale caves, collapsed caves, or caves filled with sediment (Zeng and others, 2011a, b; Zhiqian and Tailiang, 2015; Rao and Wang, 2015; Xu and others, 2016; Liu and Wang, 2017; Zhu and others, 2017). Similar anomalous bead-string reflections have been identified on some of the seismic profiles from the west and east South Miami Heights 3D seismic surveys (fig. 1) and are also interpreted to represent seismic-scale caves or paleocaves (Klimchouk and Ford, 2000; Osborne, 2000). Paleocaves are caves that have lost their mass transport function; that is, they are decoupled from the present hydrogeochemical system (Klimchouk and Ford, 2000). Identification of caves on seismic profiles is important, because they could affect, at least locally, the groundwater flow system of the Floridan aquifer system in southeastern Florida. It has been suggested that caves are an important part of carbonate petroleum reservoir systems in the Tarim Basin (Zeng and others, 2011a, b; Zhiqian and Tailiang, 2015; Xu and others, 2016; Liu and Wang, 2017; Zhu and others, 2017). At the study area, in some cases, sagging seismic reflections overlying bead-string reflections suggest the caves have collapsed, and elsewhere, where no overlying seismic-reflection sag is present, it is possible the cave cavities or sediment-filled cave cavities are intact. Because it is not known whether the bead-string reflections, in all cases, represent collapsed caves, sediment-filled caves, or intact cave cavities, the anomalies will be referred to herein simply as "caves," indicated with quotation marks.

For the shallow-marine cyclic carbonate strata of the Floridan aquifer system in southeastern Florida, Cunningham and others (2018) reported that commonly, at several hierarchical scales, the upper part of depositional cycles, are characterized by higher permeability, as compared to the lower part of the cycles. The higher permeability located at the uppermost part of cycles is generally produced by subaerial exposure at the upper boundaries of cycles and the associated formation of secondary porosity by epigenic karst (compare to Budd and others, 1995); that is, the acidic dissolution of carbonate rock (in this case) by water recharged from the surface (Klimchouk and Ford, 2000). The upper boundaries of the seismic sequences and depositional sequences O1, O3, AP1, and AP3 (fig. 2) correspond to the upper surface, or approximate the upper surface, of four major permeable units present within the Floridan aquifer system in southeastern Florida: the Boulder Zone, the uppermost permeable zone

of the Lower Floridan aquifer, and the Avon Park permeable zone, and to a greater extent, an approximation of the top of the Upper Floridan aquifer, respectively (fig. 2). The upper boundaries of the seismic sequences O1, O3, AP1, and AP3 are equivalent, or approximately equivalent, to the seismic horizons O1, O3, AP1, and AP3 (fig. 2). In this section, maps of the four seismic horizons are presented and described, and the seismic and karst characteristics of the seismic-sag structures and bead-string reflections in the study area are described.

Seismic Sequence O1

The structural altitude maps and time-structure maps shown in figures 8-12 were generated for seismic horizon O1, which is equivalent or generally equivalent to the tops of seismic sequence O1, depositional sequence O1, and the highly permeable Boulder Zone (fig. 2). The maps of the seismic horizon O1 show that the paleotopography of the upper bounding surface of seismic sequence O1 is rugged and disturbed because of karst collapse, faulting, and fracturing at and below the surface (figs. 8-12). These processes are mainly attributed to intense early Eocene epigenic and later-stage hypogenic karstification. Seismic-sag structures typically manifest as structural depressions with a semicircular-planform shape commonly trending along fault-trace images (figs. 8, 9, 11, 12). The lower part of the seismic-sag structures exhibits an area of cave collapse or cave stoping (upward void migration caused primarily by the mechanical process of ceiling collapse, Field, 2002; Hess, 2005) or both; for example, the lower part of seismic-sag structure S3 in figure 13. The upper zone is characterized by vertically stacked, concave-upward arrangements of generally parallel seismic-reflection patterns that typically extend upward from the lower zone of more sagging, disturbed, or chaotic seismic reflections (Fig. 13). As discussed later, bead-string reflections or evidence for “caves” are typically associated with the columniform seismic-sag structures and faults, such as at the seismic-sag structures S14 and S15 (fig. 14). The roots of the columniform seismic-sag structures typically are within seismic sequence O1, or in some cases, possibly below it (figs. 13, 14) Because of decreasing seismic resolution with depth, the inferred locations for the roots of the deeper collapses are tentative. The columniform seismic-sag structures labeled in figure 8 almost all unambiguously extend upward beyond the top of seismic sequences O1 and O3. Seismic-sag structures rooted in O1 or below and that extend upward past the upper boundary of seismic sequences AP1, or beyond, such as seismic-sag structure S3 in figure 13, were produced during deep-burial cave collapse or cave stoping or both (Field, 2002; Hess, 2005), and consequent subsidence and sag of an overlying column of overburden (compare to, Zuo and others, 2009). The extreme height of some of the columnar structures (as much as 2,700 ft) suggests a long-term interplay between collapse, stoping, columnar subsidence, and hypogenic karstification within the columns. Similar hypogenic karst has also been documented in the carbonate rocks of the Floridan aquifer system in Broward County (fig. 1*A*) by Cunningham and others (2018). Some seismic structures that show collapse do not extend upward beyond the upper boundary of seismic horizon O1. These structures presumably formed entirely during subaerial exposure of the upper boundary of depositional sequence O1 and are a result of epigenic karstification.

In figures 11 and 12, the respective seismic data volumes of the west and east South Miami Heights seismic surveys show an abundance of fault-trace images of the thinned-fault-likelihood attribute within seismic sequence O1. The fault-trace images of the thinned-fault-likelihood attribute and, commonly, locations where they intersect (figs. 11, 12) are typically associated with structural lows related to karst collapse, suggesting faults likely concentrate fluid flow related to karst dissolution of the carbonate rock. Faults and fractures related to karst collapse are also confirmed to be common within the dolomite and limestone of depositional sequence O1 by borehole image data from test well G-3990 (for example, fig. 13*C*).

Seismic Sequence O3

The structural altitude maps and time-structure maps shown in figures 15-19 were generated for seismic horizon O3, which is equivalent or generally equivalent to the tops of seismic sequence O3, depositional sequence O3, and the uppermost major permeable zone of the Lower Floridan aquifer (fig. 2). As with the upper surface of seismic sequence O1, the upper surface of seismic sequence O3 is rugged because of collapse, faulting, and fracturing at and below the surface (figs. 15-19). These processes are interpreted to be mainly associated with intense early Eocene epigenic and later-stage hypogenic karstification. Seismic-sag structures S1 to S20 at the upper surface of the seismic sequence O3 (fig. 15) commonly trend along fault-trace images produced by the thinned-fault-likelihood attribute. A semicircular planform shape common to the area of sag width (“where the shape of the subsidence profile changes from concave to convex,” McDonnell and others, 2007) of the seismic-sag structures is represented in horizontal similarity slices of the seismic data volumes (for example, figs. 13*D* and 14*B*, *C*). The low similarity-attribute rings outlining the outer diameter (indicated by red circles in figs. 13*D* and 14*B*, *C*) of the sag-width areas in the similarity slices in figures 13*D* and 14*B, C* are coincident with faults (yellow lines on figs. 13*D* and 14*B*, *C*). This relationship between low similarity rings on similarity slices and faults on seismic profiles indicates that it is common for ring faults (Bertoni and Cartwright, 2005) to occur within seismic-sag structures and to bound pipe-like structures within the lower part of many seismic-sag structures, such as in seismic-sag structures S14 and S15 in figure 14. Similar relationships between semicircular, low continuity and coherency attributes and columniform karst-collapse structures have been identified in other ancient carbonate platforms (Zeng and others, 2011a, fig. 13; Sun and others, 2013). Cave-roof stoping (Waltham, 2002) may well play a role in the formation of the South Miami Heights pipe-like structures.

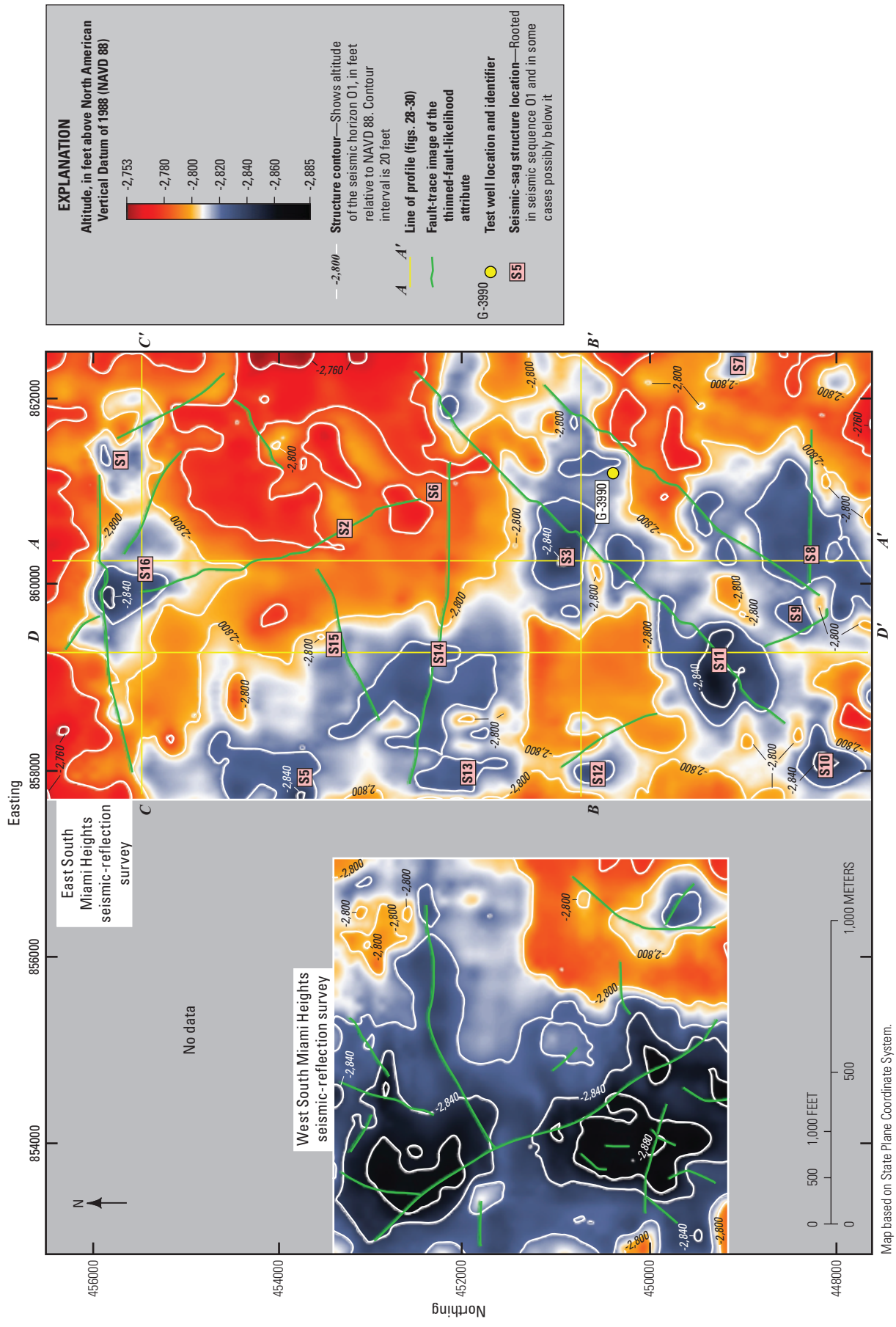

Figure 8. Structural altitude maps of seismic horizon O1 at the west and east South Miami Heights three-dimensional (3D) seismic survey areas (fig. 1).

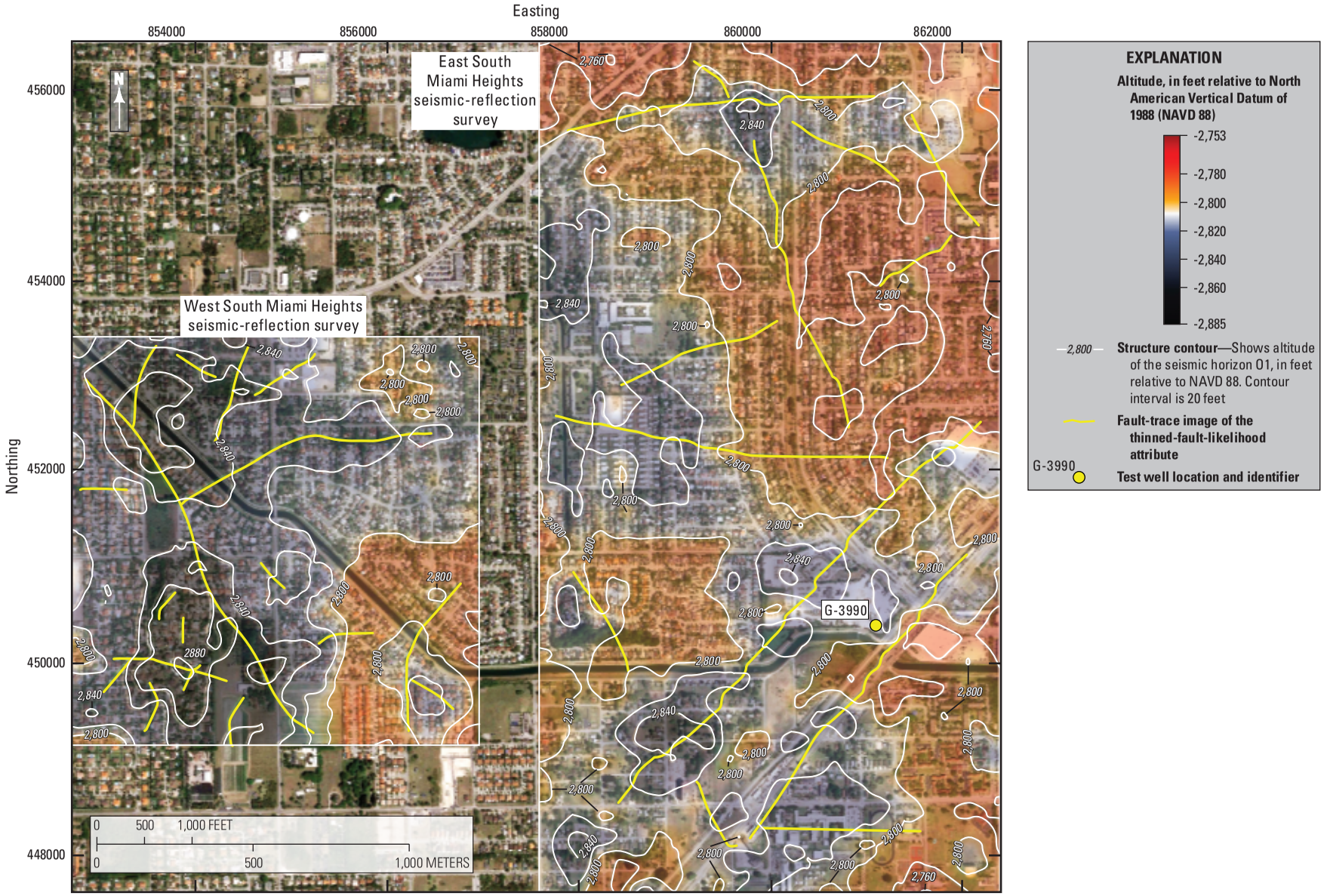

Base map data from Google, 2017.
Map based on State Plane Coordinate System.
Florida East 901 in U.S. Survey feet.
North American Datum of 1983

Figure 9. Structural altitude maps of seismic horizon O1 at the west and east South Miami Heights three-dimensional (3D) seismic survey areas (fig. 1) overlain on an aerial image. The aerial imagery is included to show the relationship of the structural altitude map to the dense suburban development in the study area.

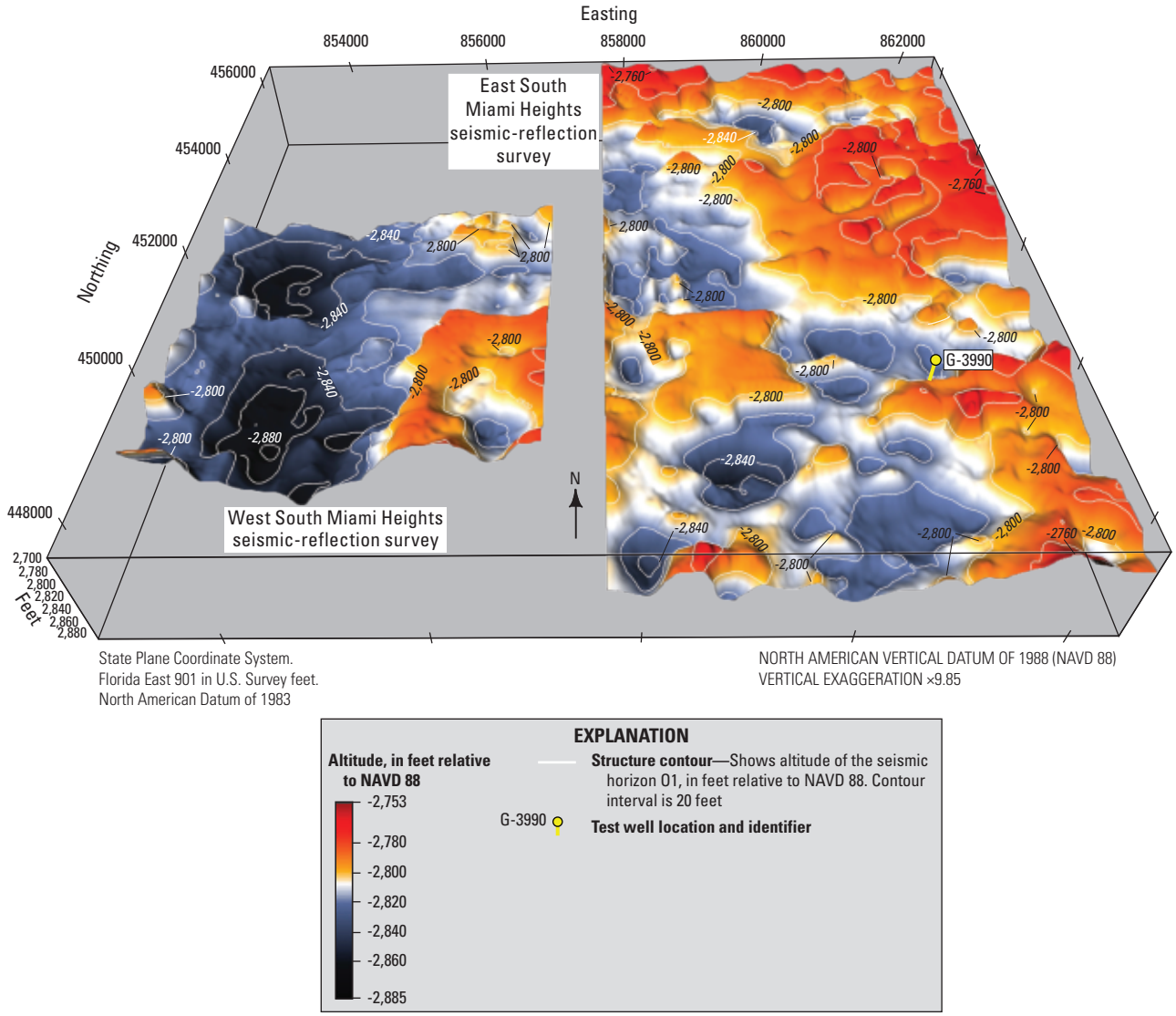

Figure 10. Oblique view, looking north, of three-dimensional (3D) structural altitude maps of seismic horizon O1 at the west and east South Miami Heights 3D seismic survey areas.

As for seismic sequence O1, the upper parts of seismic-sag structures in seismic sequence O3 exhibit vertically stacked, concave-upward arrangements of generally parallel seismic-reflection patterns. The seismic-sag structures extending upward past the upper boundary of seismic sequence O3 are interpreted to have been produced during deep burial by cave collapse or cave stoping or both, and associated overburden subsidence (compare to, Zuo and others, 2009), and later dissolution by chemically aggressive water (Monroe, 1972) during hypogenic cross-formational fluid flow. Structural lows, which are not associated with columniform seismic-sag structures extending upward above seismic horizon O3, are likely related to epigenic karst during subaerial exposure of the depositional sequence boundary O3 and, in some cases, extend downward beyond the top of the seismic horizon O1.

In figures 18 and 19, the respective seismic data volumes of the west and east South Miami Heights seismic surveys show an abundance of fault-trace images of the thinned-fault-likelihood attribute within the seismic sequence O3. The fault-trace images of the thinned-fault-likelihood attribute are somewhat less abundant than those on the depositional sequence O1 seismic data volumes (figs. 11, 12). This difference in abundance reflects a less prominent overprint of epigenic karstification and later stage hypogenic karstification on the carbonate rocks of the seismic sequence O3 compared to the overprint on the carbonate rocks of seismic sequence O1.

Seismic Sequence AP1

The structural altitude maps and time-structure maps shown in figures 20-24 were generated for seismic horizon AP1, which is equivalent or generally equivalent to the tops of seismic sequence AP1, depositional sequence AP1, and the Avon Park permeable zone (fig. 2). The maps of the seismic horizon AP1 indicate

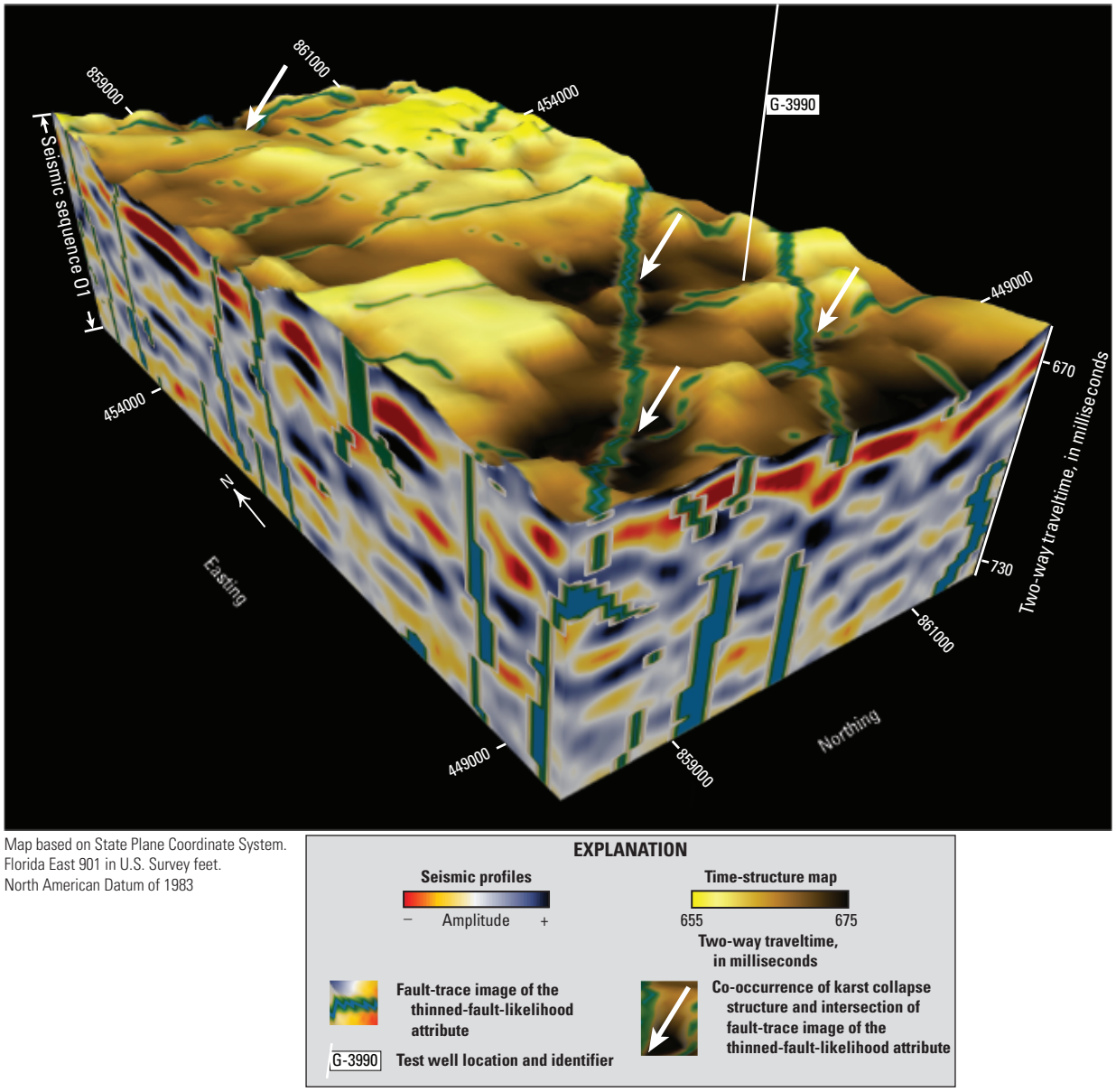

Figure 11. Seismic data volume of the east South Miami Heights three-dimensional (3D) seismic survey, including a time-structure map of seismic horizon O1 as the top surface and the approximate position of seismic horizon CK as the base (fig. 2). The volume approximates the entire thickness of seismic sequence O1 (fig. 2). The west side of the volume is a seismic profile along the inline direction, and the south side is a seismic profile along the crossline direction. Fault-trace images of the thinned-fault-likelihood attribute are shown along the sides and the upper seismic time-structure map.

relatively low and broad paleotopographic relief of the upper boundary of seismic sequence AP1 as compared to structural altitude maps of seismic horizons O1 and O3 (figs. 10, 17, 22). Eight seismic-sag structures intersect the top of seismic horizon AP1 (S1-S6, and S18-S19, fig. 20) and each are rooted within seismic sequence O1 or O3, and in some cases possibly deeper. Four of the eight seismic-sag structures terminate upward within the upper part of the Arcadia Formation (for example, fig. 13). The eight seismic-sag structures have produced semicircular structural depressions on the seismic horizon AP1 (fig. 20).

As shown in figures 13 and 25, columniform seismic-sag structure S3 exhibits an upper zone of sagging suprastratal deformation (compare to Loucks, 1999) composed of vertically stacked, concave-upward arrangements of generally parallel seismic-reflection patterns. As discussed later herein (figs. 13, 14, 25), bead-string reflections representing “caves” are present within seismic sequence AP1, and most are associated with faults or columniform seismic-sag structures. The seismic horizon AP1 intersects all the seismic-sag structures shown on figure 20 within the upper zone of sagging suprastratal deformation (for example S3, fig. 13).

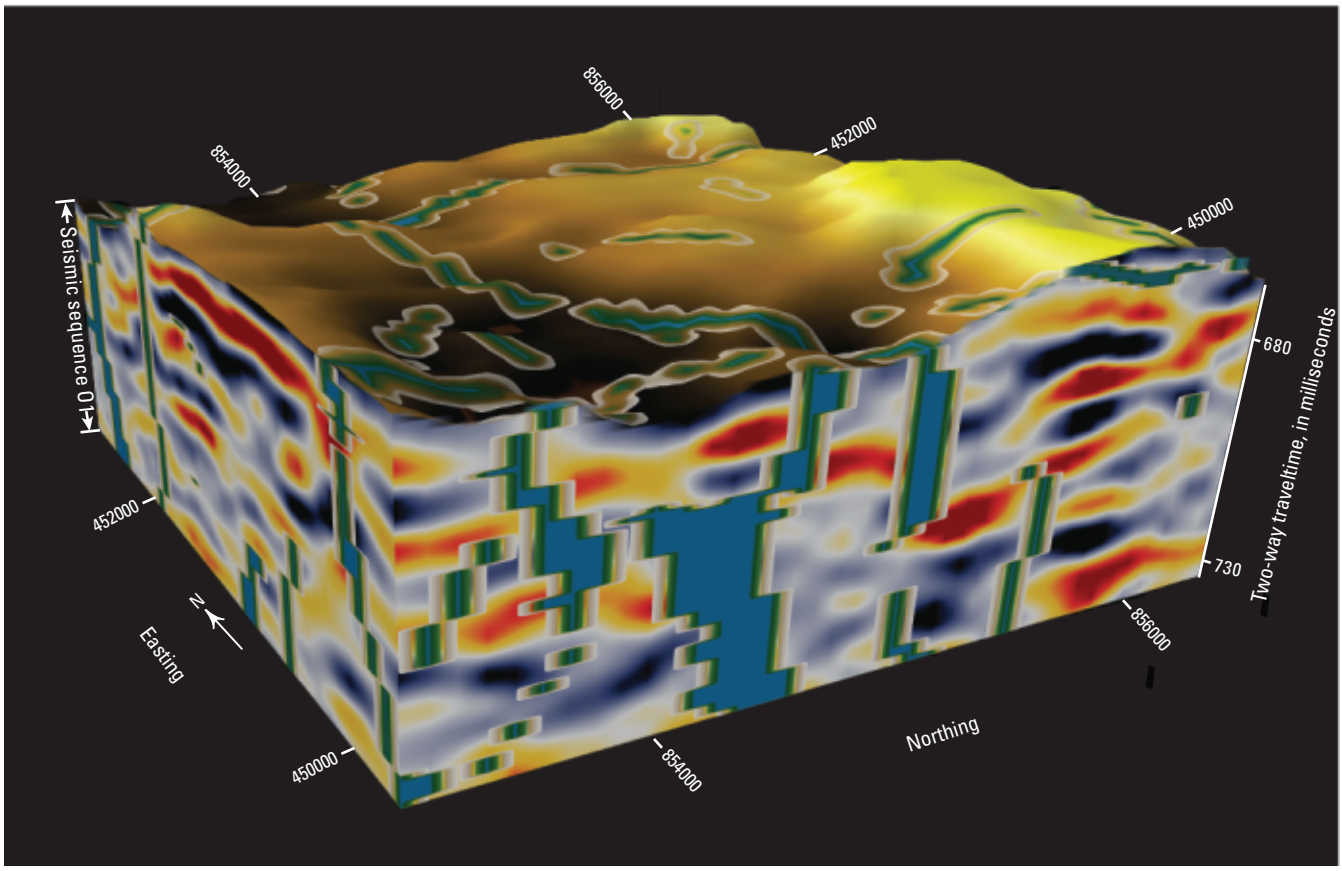

Map based on State Plane Coordinate System.
Florida East 901 in U.S. Survey feet.
North American Datum of 1983

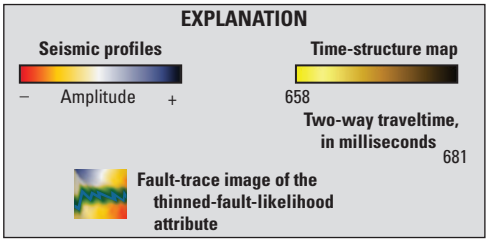

Figure 12. Seismic data volume of the west South Miami Heights three-dimensional (3D) seismic survey, including a time-structure map of the seismic horizon O1 as the top surface and the approximate position of seismic horizon CK as the base (fig. 2). The volume approximates an entire thickness of seismic sequence O1 (fig. 2). The west side of the volume is a seismic profile along the inline direction, and the south side is a seismic profile along the crossline direction. Fault-trace images of the thinned-fault-likelihood attribute are shown along the sides and the upper seismic time-structure map.

The spatial density of the fault-trace images of the thinned-fault-likelihood attribute is greater within seismic sequences O1 and O3 (figs. 11, 12, 18, 19) than within seismic sequence AP1 (figs. 23, 24). This difference in the spatial density of fault-trace images reflects a more pronounced seismic-scale overprint of epigenic and hypogenic karst on the carbonate rock of seismic sequences O1 and O3 compared to any karstic overprinting on the carbonate rock of seismic sequence AP1. Although evidence has not been thoroughly investigated, it cannot be ruled out that tectonic stresses, and regional faulting and fracturing could have been more intense following deposition of the lower Eocene Oldsmar Formation (seismic sequences O1-O3) than during and after the middle Eocene. Alternatively, mechanical stratigraphy could play a role in fracture spatial density differences between seismic sequences O1 and O3, and seismic sequence AP1 (Morettini and others, 2005). At a gross scale, brittle deformation is common for dolomite in the Oldsmar Formation but uncommon for limestone in the overlying middle Eocene Avon Park Formation, and thus, the dolomite of the Oldsmar Formation would be more susceptible to fracturing as compared to the limestone of the Avon Park Formation.

Seismic Sequences AP2 and AP3

Overlying the seismic sequence AP1 are the two seismic sequences AP2 and AP3 (fig. 2). The structural altitude maps and time-structure maps shown in figures 26-30 were

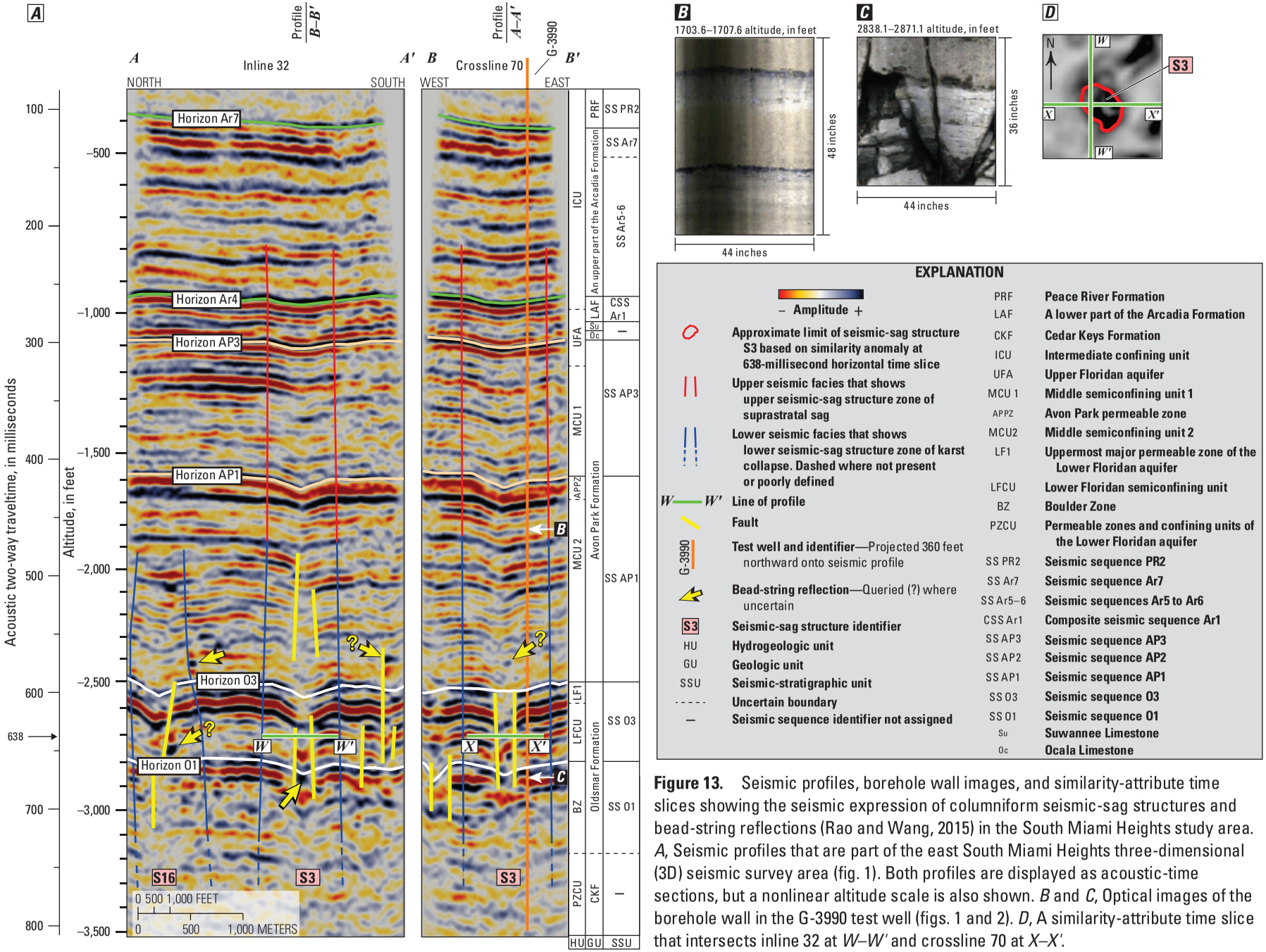

Figure 13. Seismic profiles, borehole wall images, and similarity-attribute time slices showing the seismic expression of columniform seismic-sag structures and bead-string reflections (Rao and Wang, 2015) in the South Miami Heights study area. *A*, Seismic profiles that are part of the east South Miami Heights three-dimensional (3D) seismic survey area (fig. 1). Both profiles are displayed as acoustic-time sections, but a nonlinear altitude scale is also shown. *B* and *C*, Optical images of the borehole wall in the G-3990 test well (figs. 1 and 2). *D*, A similarity-attribute time slice that intersects inline 32 at *W*–*W*′ and crossline 70 at *X*–*X*′.

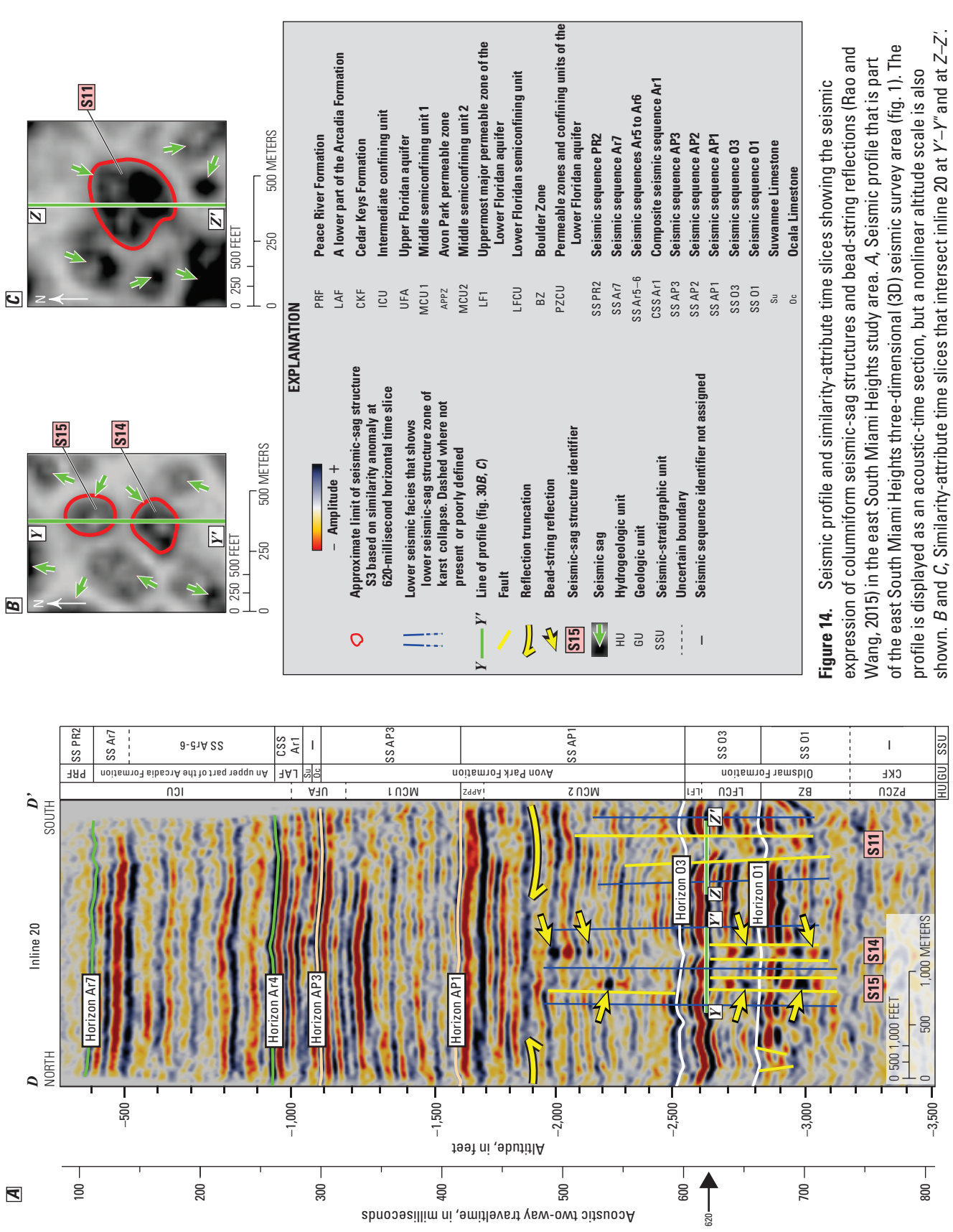

Figure 14. Seismic profile and similarity-attribute time slices showing the seismic expression of columniform seismic-sag structures and bead-string reflections (Rao and Wang, 2015) in the east South Miami Heights study area. *A*, Seismic profile that is part of the east South Miami Heights three-dimensional (3D) seismic survey area (fig. 1). The profile is displayed as an acoustic-time section, but a nonlinear altitude scale is also shown. *B* and *C*, Similarity-attribute time slices that intersect inline 20 at *Y*′–*Y*″ and at *Z*–*Z*′.

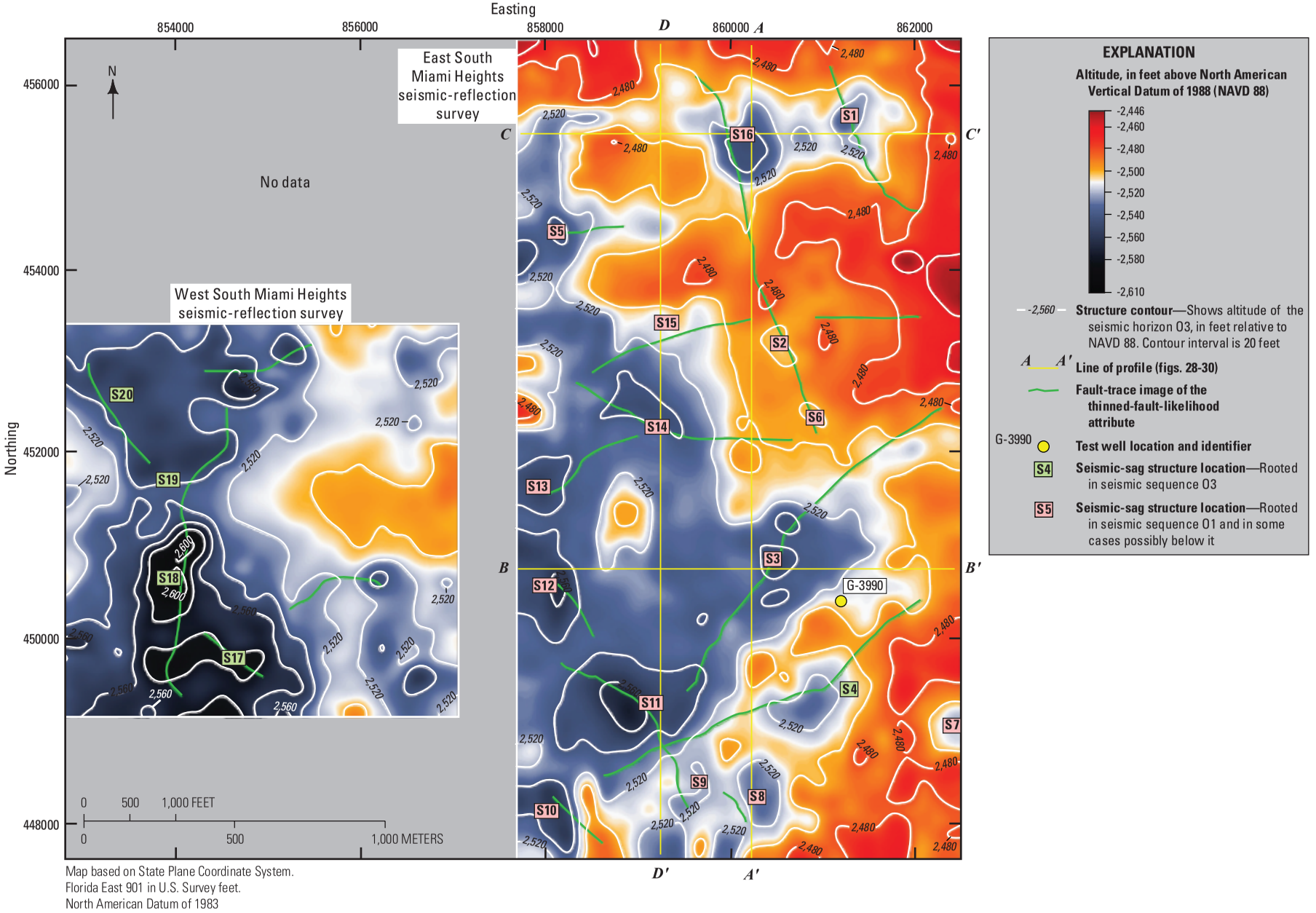

Figure 15. Structural altitude maps of seismic horizon O3 at the west and east South Miami Heights three-dimensional (3D) seismic survey areas (fig. 1).

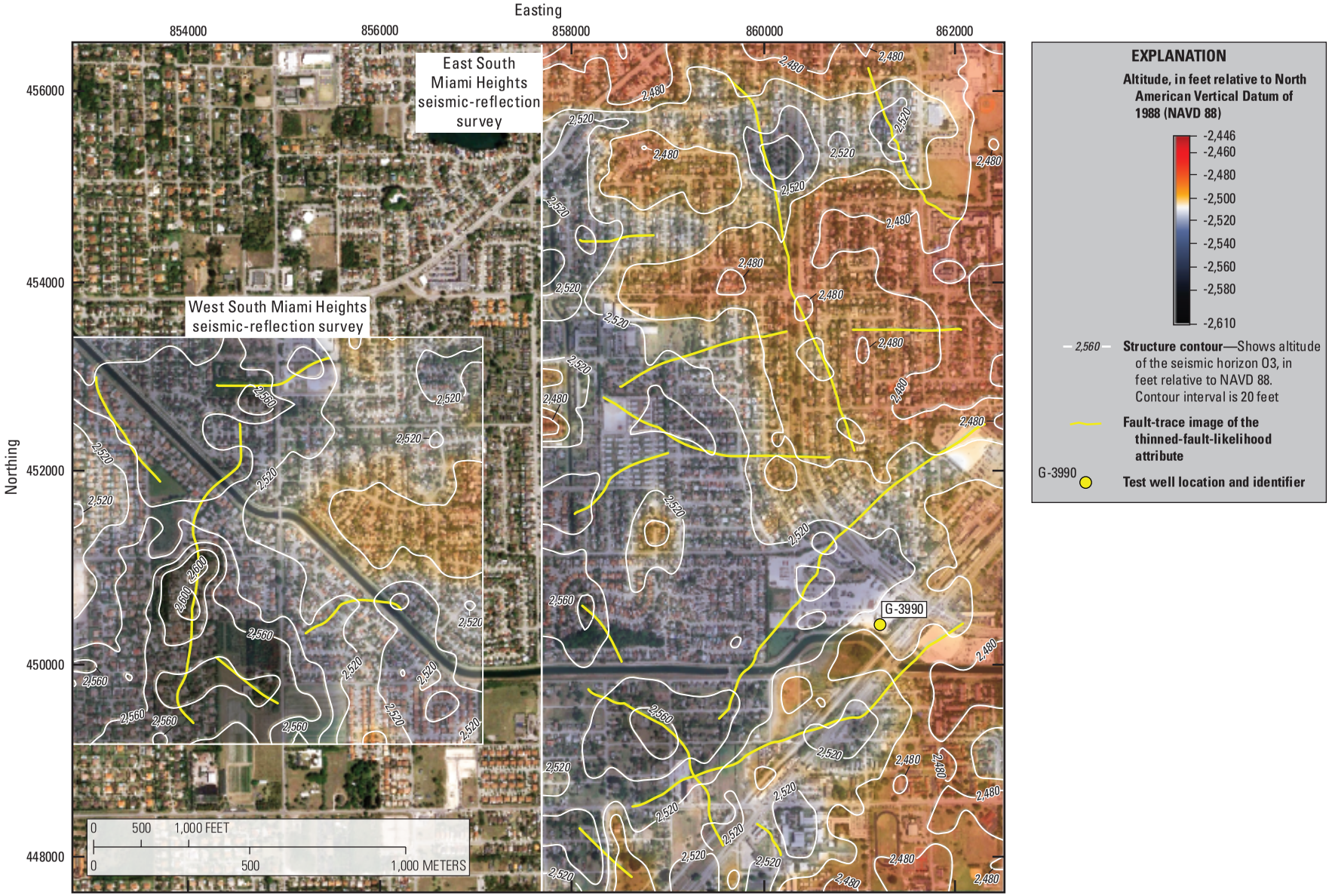

Base map data from Google, 2017.
Map based on State Plane Coordinate System.
Florida East 901 in U.S. Survey feet.
North American Datum of 1983

Figure 16. Structural altitude maps of seismic horizon O3 at the west and east South Miami Heights three-dimensional (3D) seismic survey areas (fig. 1) overlain on an aerial image. The aerial imagery is included to show the relationship of the structural altitude map to the dense suburban development in the study area.

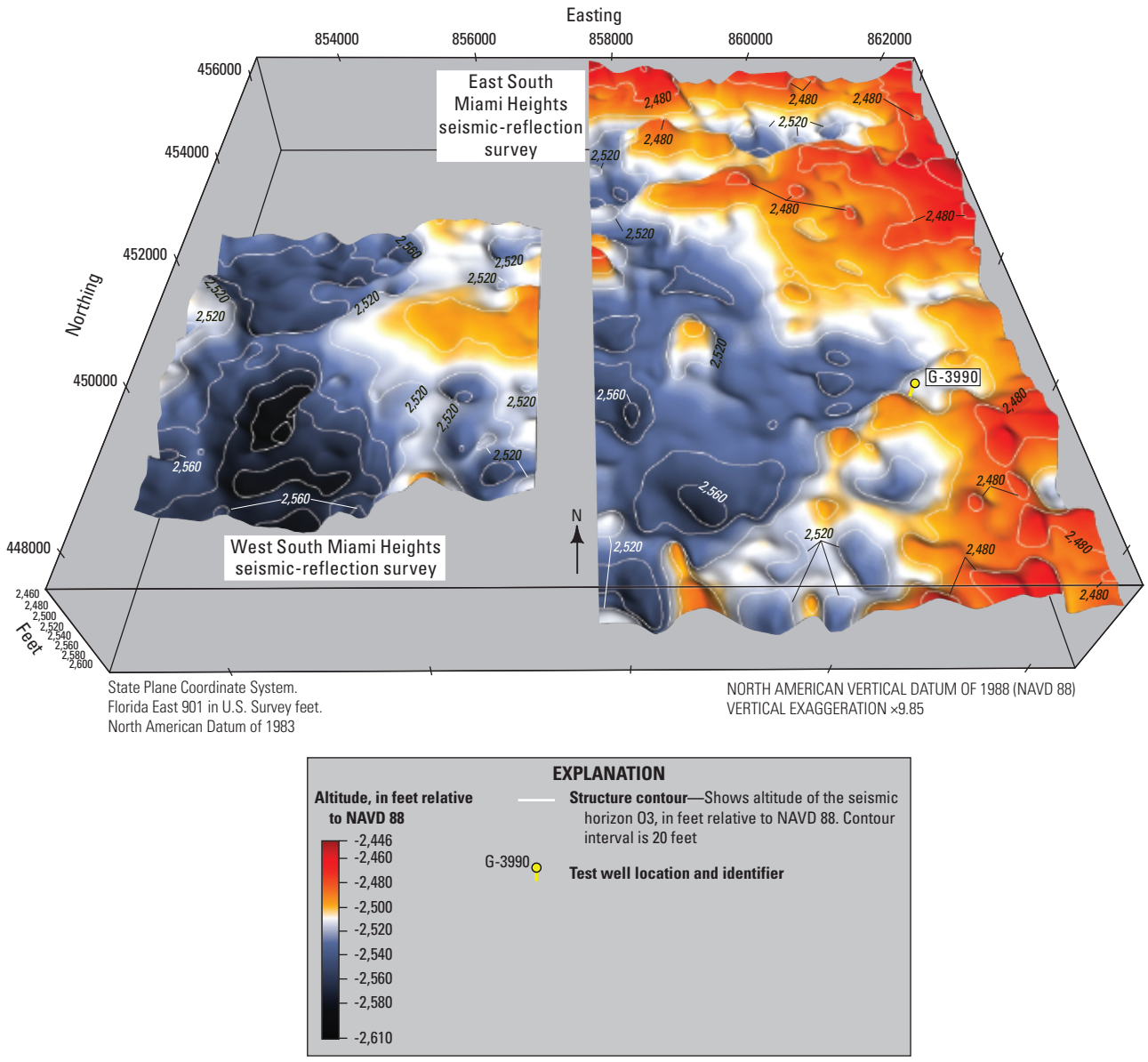

Figure 17. Oblique view, looking north, of three-dimensional (3D) structural altitude maps of seismic horizon O3 at the west and east South Miami Heights 3D seismic survey areas (fig. 1).

generated for seismic horizon AP3, which is equivalent or generally equivalent to the tops of seismic sequence AP3 and depositional sequence AP3, and to a greater extent, an approximation of top of the Upper Floridan aquifer (fig. 2). The mapping of seismic horizon AP3 indicates relatively low and broad paleotopographic relief compared to that of the upper surfaces of seismic sequences O1 and O3 (figs. 10, 17, 28). The upper bounding surface of depositional sequence AP3 (fig. 2) has up to 0.7 ft of borehole-scale erosional paleotopographic relief, based on borehole wall images acquired from the G-3990 test well (fig. 1). The four seismic-sag structures identified in seismic horizon AP3 (S1-S4, fig. 26) are each rooted within seismic sequence O1 or O3, and in some cases possibly deeper, and extend upward beyond the top of seismic sequence AP3 to terminate within the upper part of the Arcadia Formation (for example, fig. 13). Like the seismic reflections of the seismic sequence AP1, those of seismic sequences AP2 and AP3 have a lower spatial density of fault-trace images of the thinned-fault likelihood attribute (figs. 29, 30) than the seismic reflections representative of the Oldsmar Formation (figs. 11, 12, 18, 19).

Columniform Seismic-Sag Structures

In the South Miami Heights study area, columniform seismic-sag structures are typically composed of two different seismic facies; namely, a lower and upper seismic facies. The lower seismic facies is characterized by parallel sagging, distorted, or chaotic reflection configurations. In many instances, the parallel reflections show offset in reflection

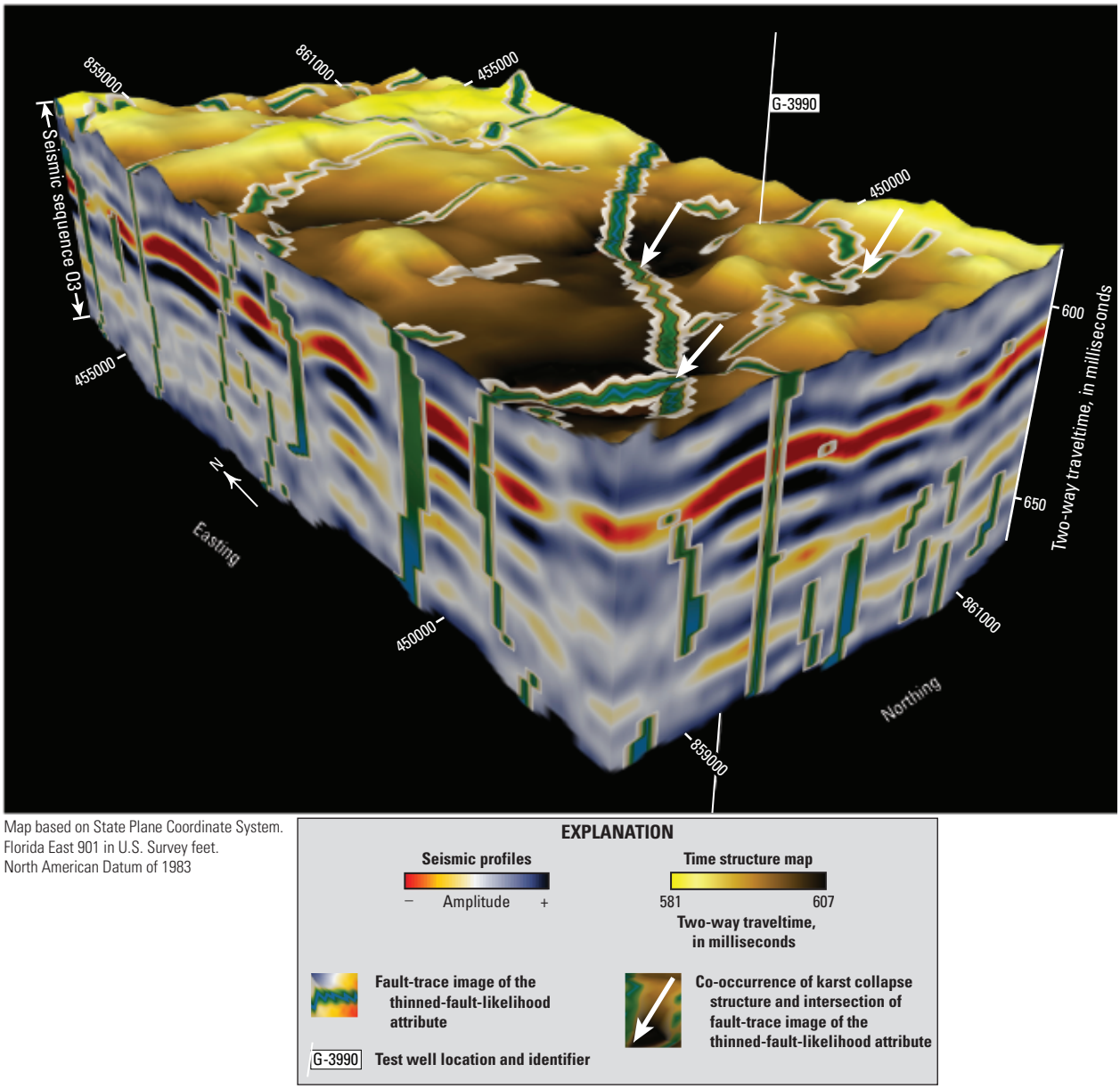

Figures 18. Seismic data volume of the east South Miami Heights three-dimensional (3D) seismic survey, including a time-structure map of the seismic horizon O3 as the top surface and a time-structure map of seismic horizon O1 as the base (fig. 2). The volume includes an entire thickness of seismic sequence O3 (fig. 2). The west side of the volume is a seismic profile along the inline direction, and the south side is a seismic profile along the crossline direction. Fault-trace images of the thinned-fault-likelihood attribute are shown along the sides and the upper seismic time-structure map.

terminations along the outer diameter of the column; the offset is indicative of faults (figs. 13, 14, 25). In some cases, anomalous bead-string reflections are present within the lower seismic facies and are interpreted as seismic-scale "caves." The lower seismic facies is interpreted to represent a columnar volume of intense karstification composed of collapsed "caves" (many may be the result of stoping), faults, and fractures. Presumably, the lower seismic facies is a columnar volume of high permeability. The upper seismic facies is composed entirely or almost entirely of continuous, parallel, sagging reflection configurations that stack vertically (figs. 13, 25). The dip of these sagging suprastratal reflections decreases upward toward the uppermost altitude and termination of the sag column. The upper seismic facies, in some cases, may also show offset in reflection terminations indicating faults along the outer diameter of the column. The upper seismic facies is interpreted to represent an area of sagging suprastratal deformation having little or no faulting, fracturing, and "caves," and to be the result of columnar overburden subsidence into accommodation space created by "cave" collapse or stoping or both, in the rocks of the lower seismic facies (compare to Loucks, 1999). The upper seismic facies is likely to have a lower permeability compared to the lower seismic facies. This interpreted difference in

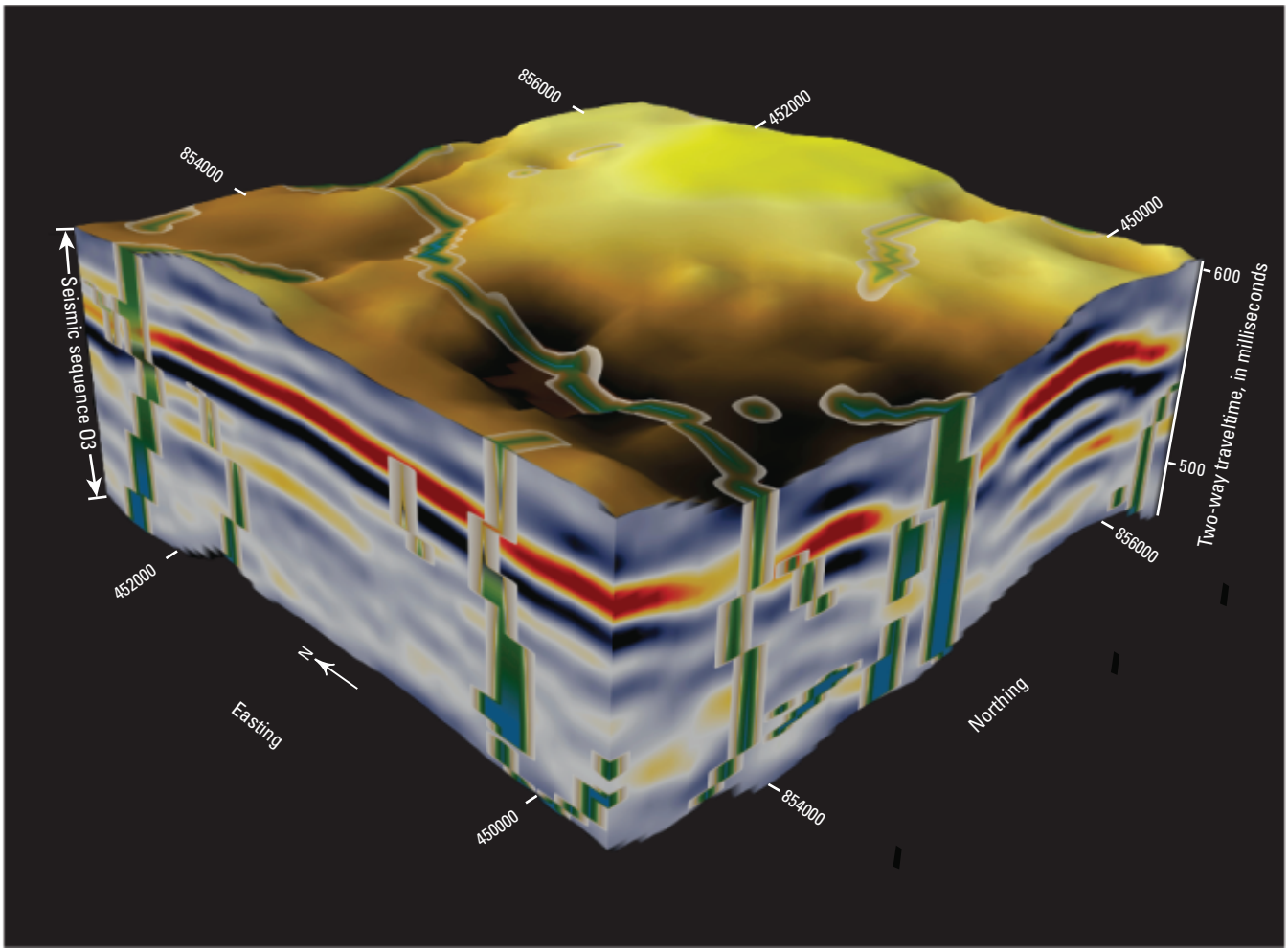

Map based on State Plane Coordinate System.
Florida East 901 in U.S. Survey feet.
North American Datum of 1983

Figures 19. Seismic data volume of the west South Miami Heights three-dimensional (3D) seismic survey, including a time-structure map of the seismic horizon O3 as the top surface and a time-structure map of seismic horizon O1 as the base (fig. 2). The volume includes an entire thickness of seismic sequence O3 (fig. 2). The west side of the volume is a seismic profile along the inline direction, and the south side is a seismic profile along a crossline direction. Fault-trace images of the thinned-fault-likelihood attribute are shown along the sides and the upper seismic time-structure map.

permeability between the rocks of the two seismic facies is inferred to be due to greater carbonate rock dissolution by chemically aggressive water and mechanical failure within the rocks of the lower seismic facies as compared to likely ductile sagging deformation within the rocks of the upper seismic facies characterized by sagging suprastratal deformation (fig. 13, seismic sag S3). The lower seismic facies only extends upward into a lower part of the Avon Park Formation below the top of depositional sequence AP1 or the top of the Avon Park permeable zone (figs. 13, 14, 25). Thus, there may be relatively higher potential for the karst-collapse structures to provide cross-formational fluid migration upward from the Boulder Zone into the lower part of the middle confining unit 2 as compared to a lower potential for cross-formational fluid migration from the upper part of the middle confining unit 2 upward to the Upper Floridan aquifer.

The seismic-reflection character and a horizontal similarity slice of a columniform seismic-sag structure is shown for S3 at the intersection of inline 32 and crossline 70 in figure 13*A*, *D*. The uppermost vertical extent of the seismic-sag structure S3 is at an acoustic two-way traveltime of about 215 ms and is in the lower part of the seismic sequences Ar5-6 (fig. 13*A*). Within the study area, the shallowest upper termination for a seismic-sag structure is

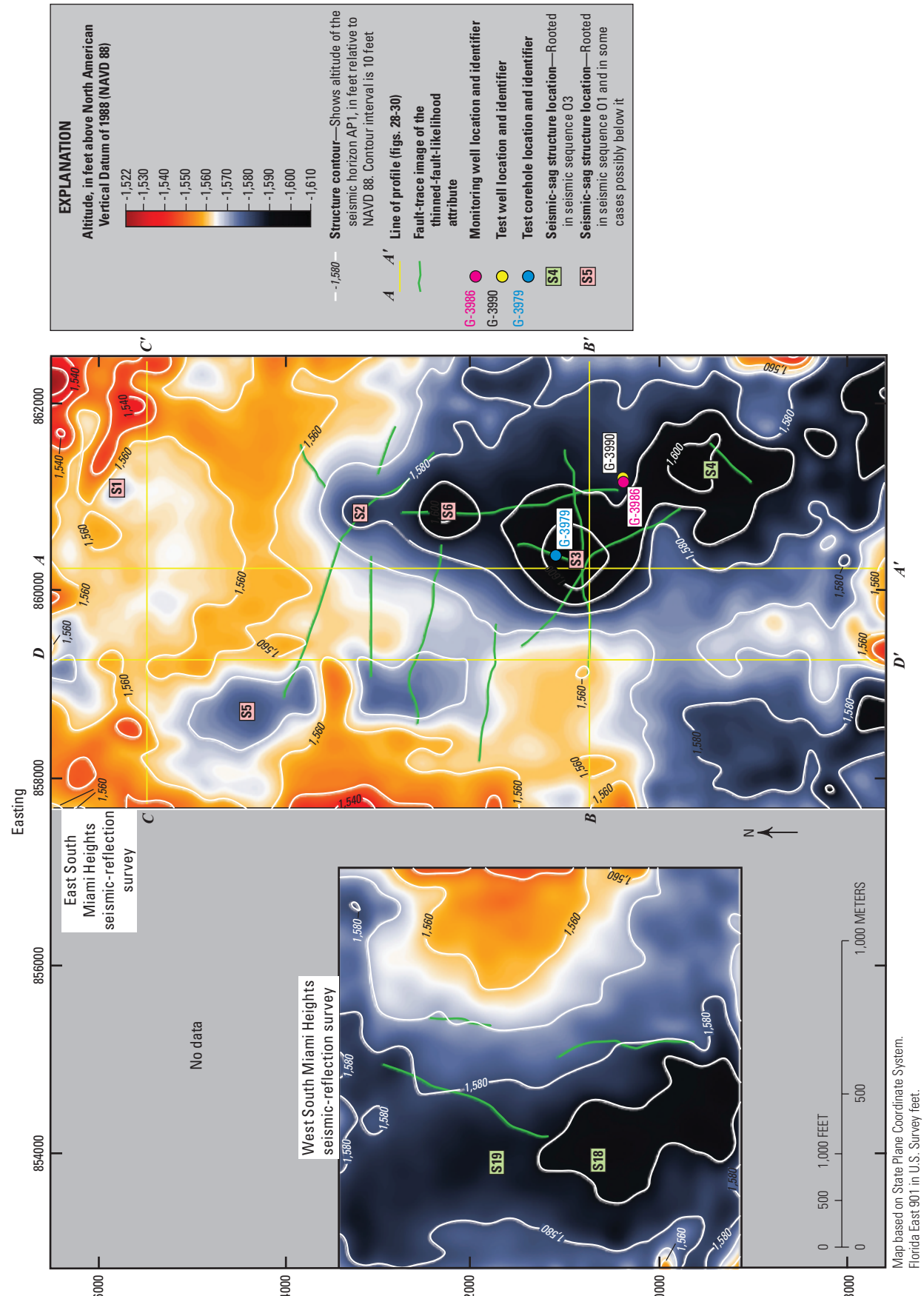

Figure 20. Structural altitude maps of the seismic horizon AP1 at the west and east South Miami Heights three-dimensional (3D) seismic survey areas (fig. 1).

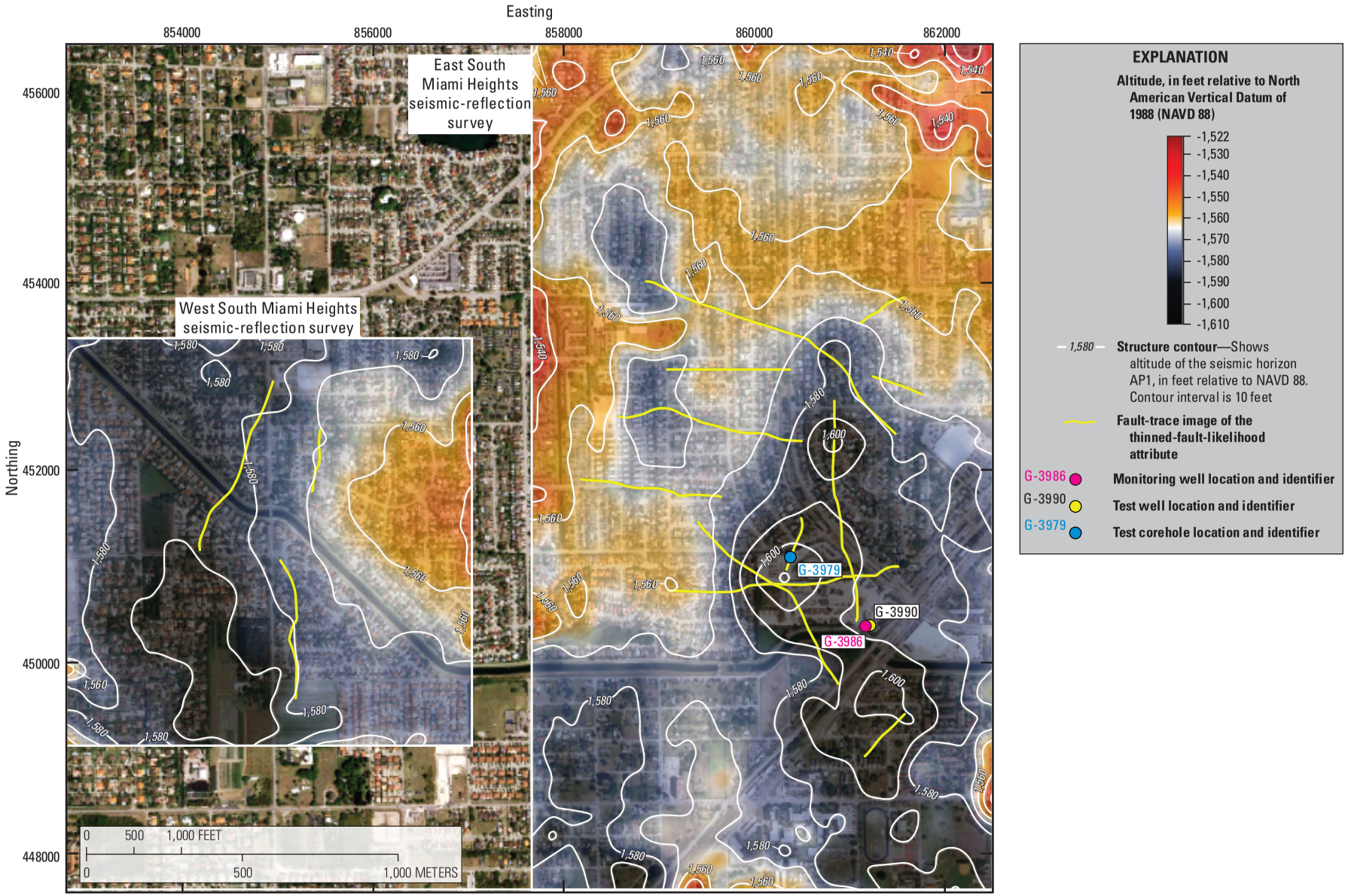

Base map data from Google, 2017.
Map based on State Plane Coordinate System.
Florida East 901 in U.S. Survey feet.
North American Datum of 1983

Figure 21. Structural altitude maps of seismic horizon AP1 at the west and east South Miami Heights three-dimensional (3D) seismic survey areas (fig. 1) overlain on an aerial image. The aerial imagery is included to show the relationship of the structural altitude map to the dense suburban development in the study area.

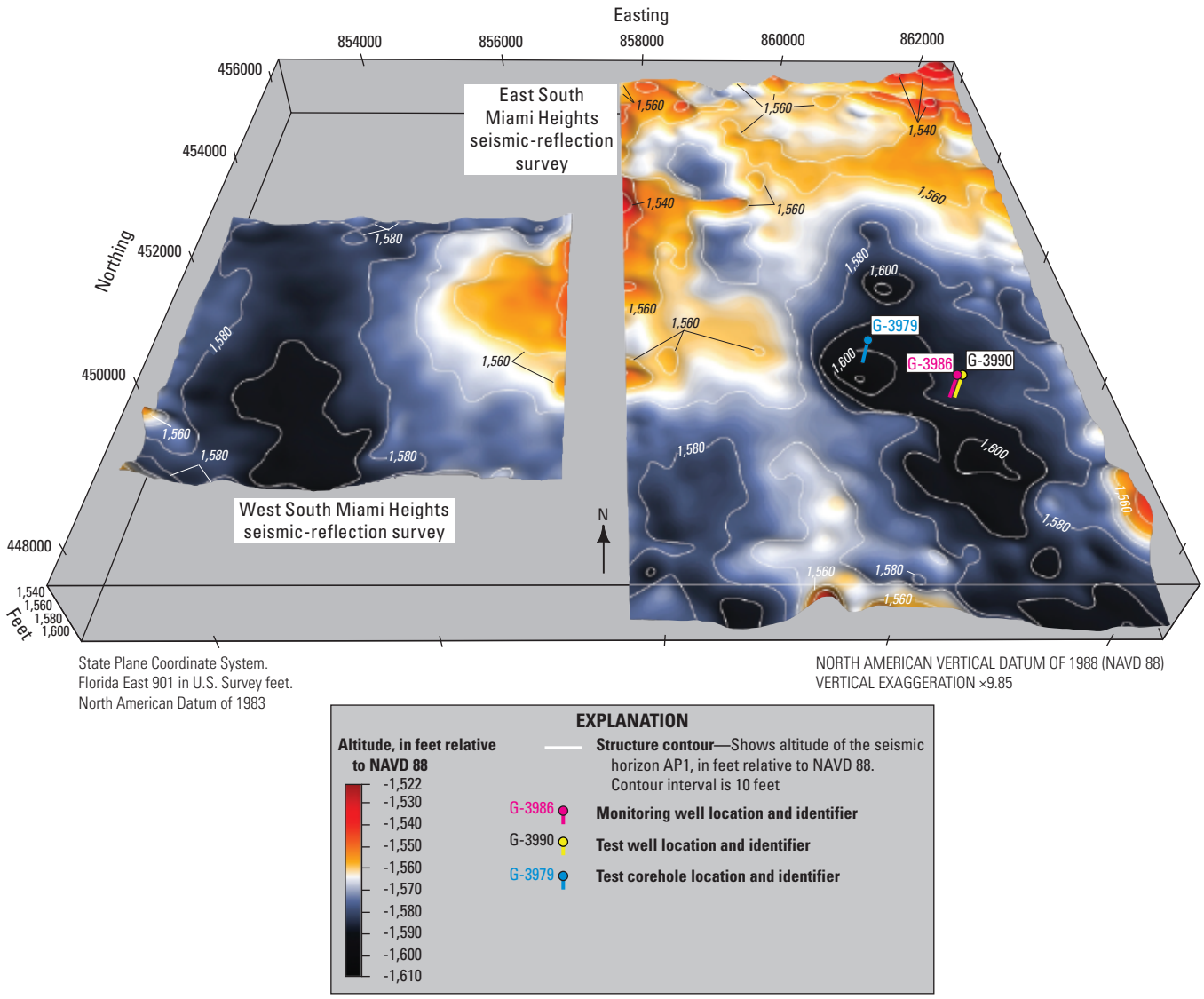

Figure 22. Oblique view, looking north, of three-dimensional (3D) structural altitude maps of seismic horizon AP1 at the west and east South Miami Heights 3D seismic reflection survey areas (fig. 1).

at sag structure S2 (fig. 26), where the uppermost vertical extent of the structure is at about 20 ms below the top of seismic sequence Ar7. The lowermost vertical extent of the columniform seismic-sag structure S3 is at an acoustic two-way traveltime of about 725 ms and is about 60 ms acoustic two-way traveltime below the seismic horizon O1 or perhaps deeper. The seismic-sag structure S3 is composed of a lower seismic facies of sagging continuous to disturbed or chaotic seismic reflections and an overlying upper seismic facies of seismic reflections exhibiting vertically stacked, concave-upward arrangements of generally parallel continuous seismic-reflection configurations (fig. 13). The lower seismic facies is interpreted to be a zone of intense karst collapse and the upper seismic facies is interpreted to be a zone of sagging suprastratal deformation. The total height of the seismic-sag structure S3 is about 2,300 ft, and the width of the seismic-sag structure at the level of the seismic horizon O3 is about 2,200 ft. The karst collapse occurred in the mesogenetic burial zone (Choquette and Pray, 1970), below depths where hydrologic processes related to the surface are effective, and during a time concurrent with deposition of the upper part of the Arcadia Formation or later. This is a span of time that includes the early to middle Miocene or later (fig. 2; Guertin and others, 2000; Cunningham and others, 2001, 2003). The production of the columniform karst-collapse structures is related to cave collapse and (or) stoping in carbonate rocks of the early Eocene Oldsmar Formation and the subsequent subsidence of columns of overburden (compare to Zuo and others, 2009). Hypogenic cross-formational flow of chemically aggressive water and dissolution of the limestone in the lower part of the Avon Park Formation is suggested by bead-string reflections (“caves”) along faults and within the upper part of the lower seismic facies of seismic-sag structures (figs. 13, 14, 25).

In figure 25, the uppermost vertical extent of columniform seismic-sag structure S16 is at an acoustic

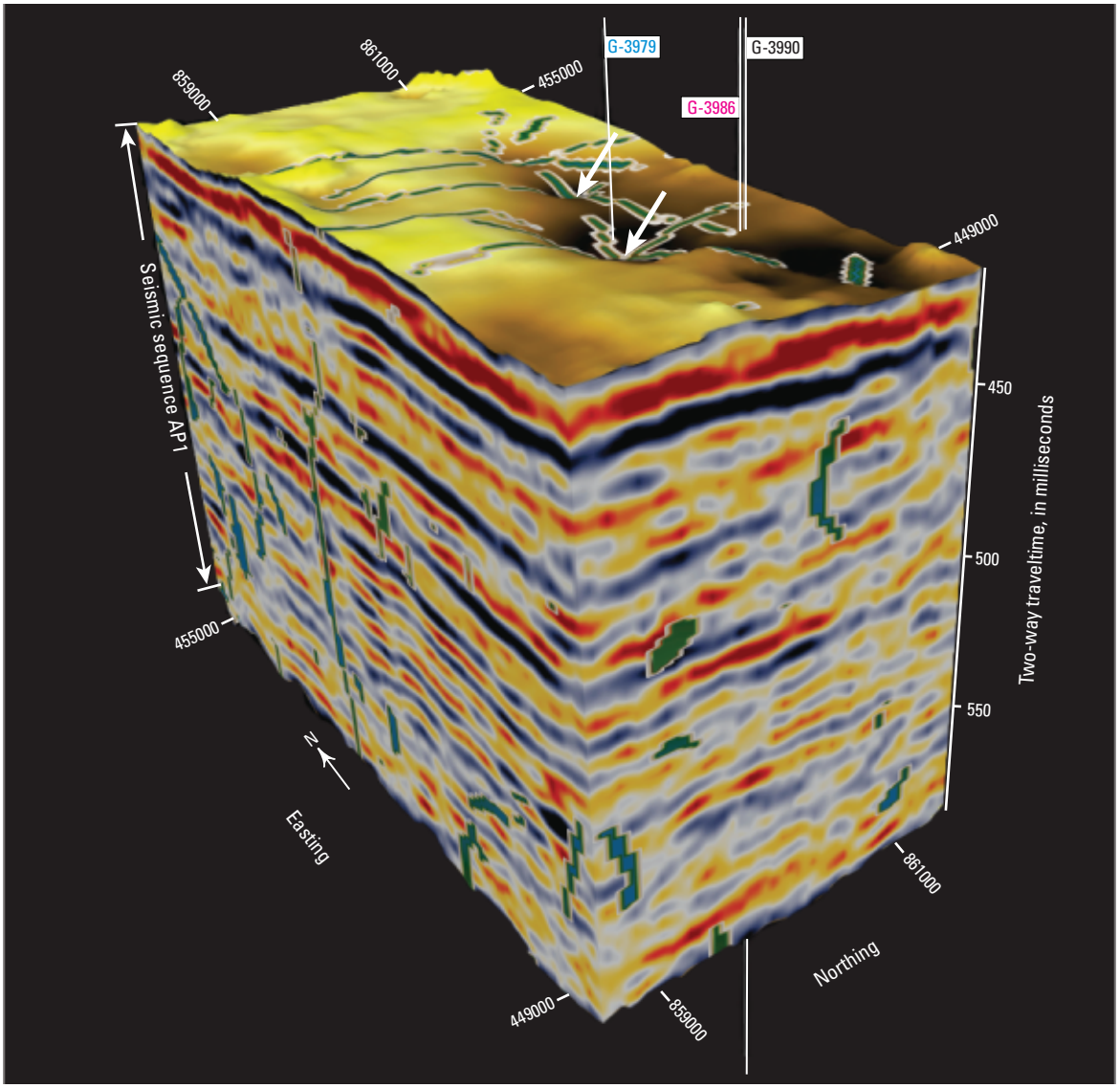

Map based on State Plane Coordinate System.
Florida East 901 in U.S. Survey feet.
North American Datum of 1983

EXPLANATION

Seismic profiles

– Amplitude +

Time-structure map

407 425

Two-way traveltime, in milliseconds

Fault-trace image of the thinned-fault-likelihood attribute

G-3986 **Monitoring well location and identifier**

G-3990 **Test well location and identifier**

G-3979 **Test corehole location and identifier**

Co-occurrence of karst collapse structure and intersection of fault-trace image of the thinned-fault-likelihood attribute

Figure 23. Seismic data volume of the east South Miami Heights three-dimensional (3D) seismic survey, including a time-structure map of the seismic horizon AP1 as the top surface and a time-structure map of seismic horizon O3 as the base (fig. 2). The volume includes an entire thickness of seismic sequence AP1 (fig. 2). The west side of the volume is a seismic profile along the inline direction, and the south side is a seismic profile along the crossline direction. Fault-trace images of the thinned-fault-likelihood attribute are shown along the sides and the upper seismic time-structure map.

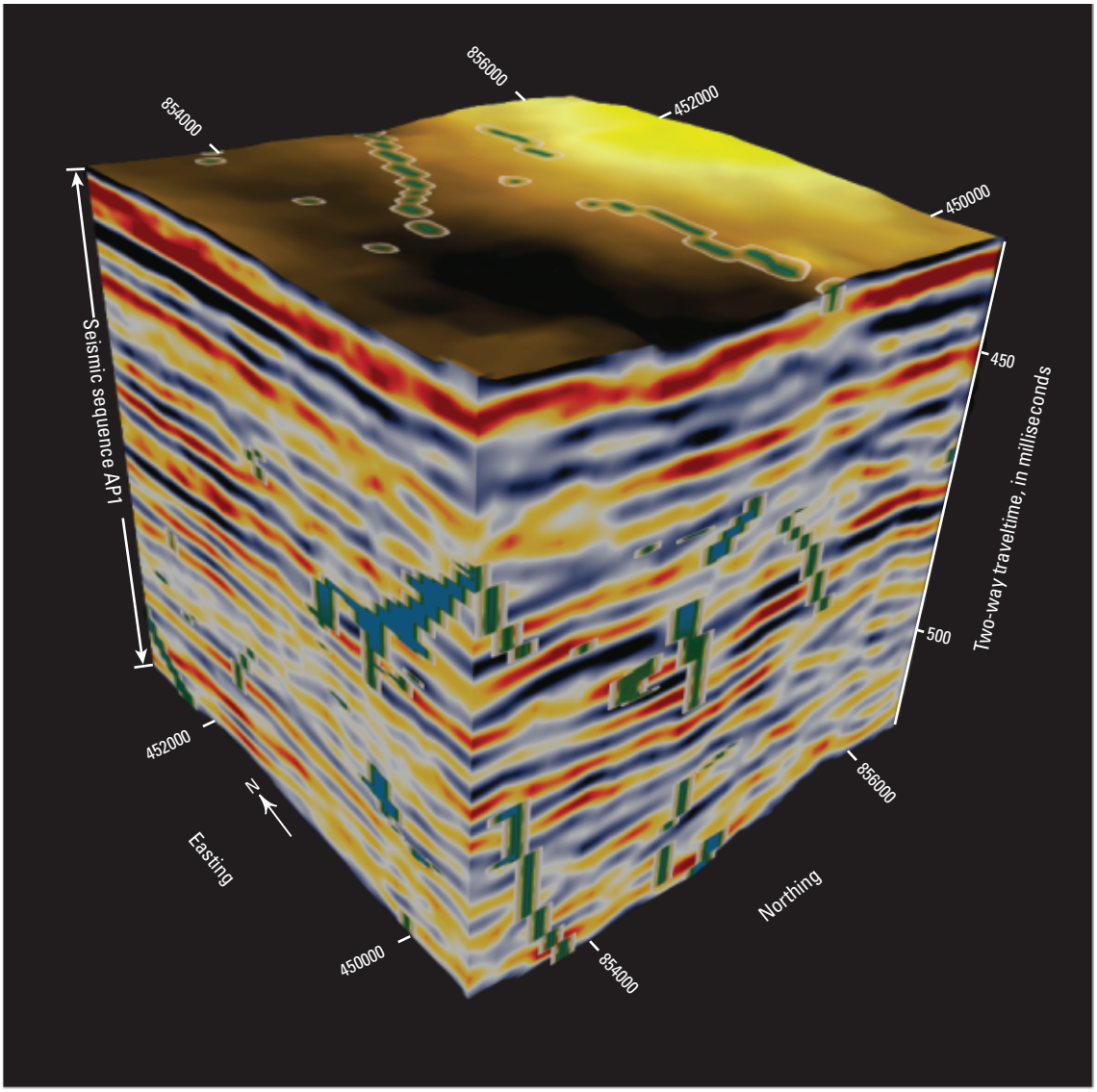

Map based on State Plane Coordinate System.
Florida East 901 in U.S. Survey feet.
North American Datum of 1983

EXPLANATION

Seismic profiles

– Amplitude +

Time-structure map

410 422

Two-way traveltime, in milliseconds

Fault-trace image of the thinned-fault-likelihood attribute

Figure 24. Seismic data volume of the west South Miami Heights three-dimensional (3D) seismic survey, including a time-structure map of the seismic horizon AP1 as the top surface and a time-structure map of seismic horizon O3 as the base (fig. 2). The volume includes an entire thickness of seismic sequence AP1 (fig. 2). The west side of the volume is a seismic profile along the inline direction, and the south side is a seismic profile along the crossline direction. Fault-trace images of the thinned-fault-likelihood attribute are shown along the sides and the upper seismic time-structure map.

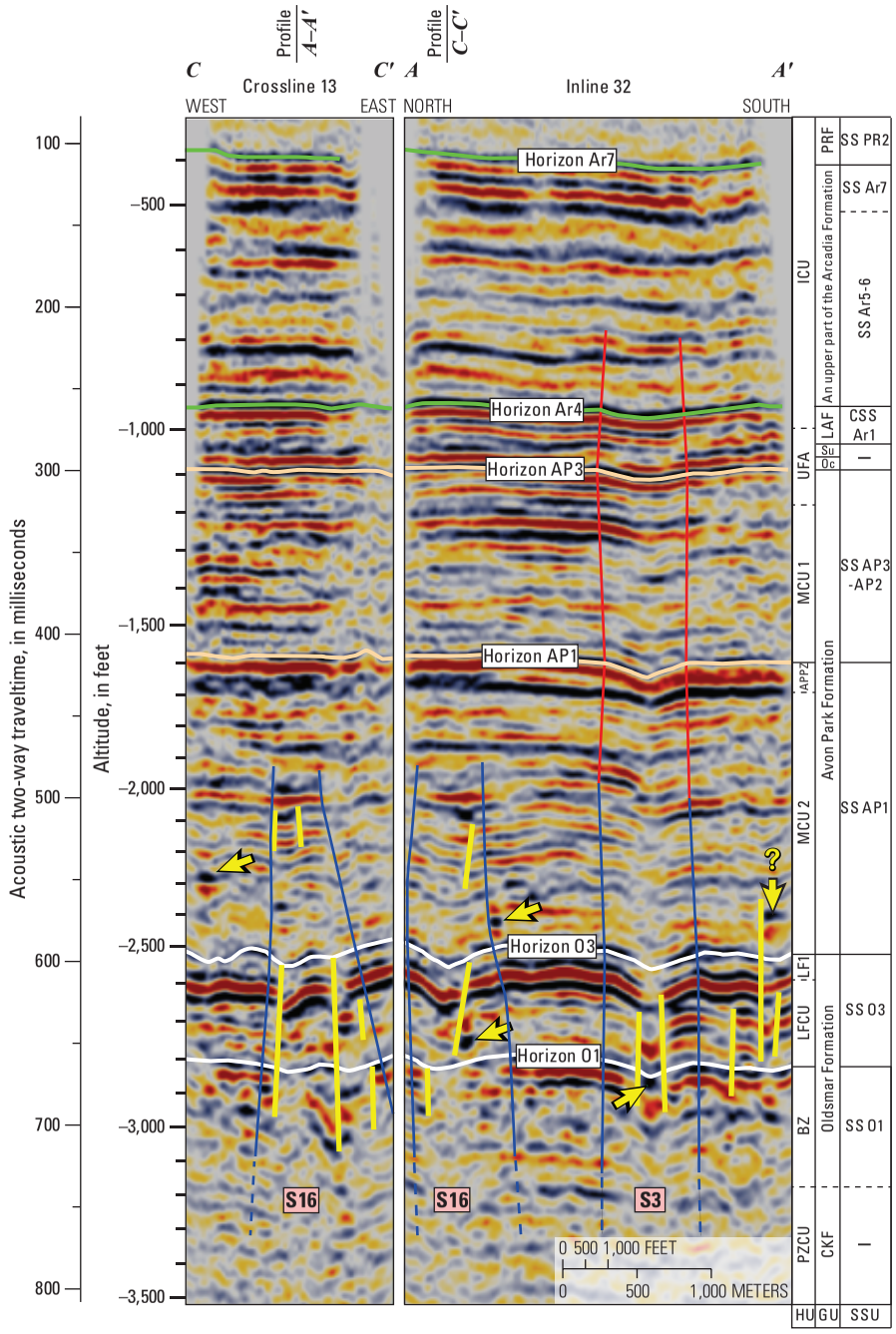

EXPLANATION

– Amplitude +

- Upper seismic facies that shows upper seismic-sag structure zone of suprastratal sag
- Lower seismic facies that shows lower seismic-sag structure zone of karst collapse. Dashed where not present or poorly defined
- Fault
- Bead-string reflection—Queried (?) where uncertain
- S3 — Seismic-sag structure identifier
- HU — Hydrogeologic unit
- GU — Geologic unit
- SSU — Seismic-stratigraphic unit
- PRF — Peace River Formation
- LAF — A lower part of the Arcadia Formation
- CKF — Cedar Keys Formation

ICU	Intermediate confining unit
UFA	Upper Floridan aquifer
MCU 1	Middle semiconfining unit 1
APPZ	Avon Park permeable zone
MCU2	Middle semiconfining unit 2
LF1	Uppermost major permeable zone of the Lower Floridan aquifer
LFCU	Lower Floridan semiconfining unit
BZ	Boulder Zone
PZCU	Permeable zones and confining units of the Lower Floridan aquifer
SS PR2	Seismic sequence PR2
SS Ar7	Seismic sequence Ar7
SS Ar5–6	Seismic sequences Ar5 to Ar6
CSS Ar1	Composite seismic sequence Ar1
SS AP3	Seismic sequence AP3
SS AP2	Seismic sequence AP2
SS AP1	Seismic sequence AP1
SS O3	Seismic sequence O3
SS O1	Seismic sequence O1
Su	Suwannee Limestone
Oc	Ocala Limestone
- - - - -	Uncertain boundary
—	Seismic sequence identifier not assigned

Figure 25. Seismic profiles showing the seismic expression of columniform seismic-sag structures S3 and S16 and bead-string reflections (Rao and Wang, 2015) in the east South Miami Heights three-dimensional (3D) seismic survey area (fig. 1). Both profiles are displayed as acoustic-time sections, but a nonlinear depth scale is also shown. The bead-string reflections, especially above horizon O3, likely indicate "caves" related to hypogenic karst.

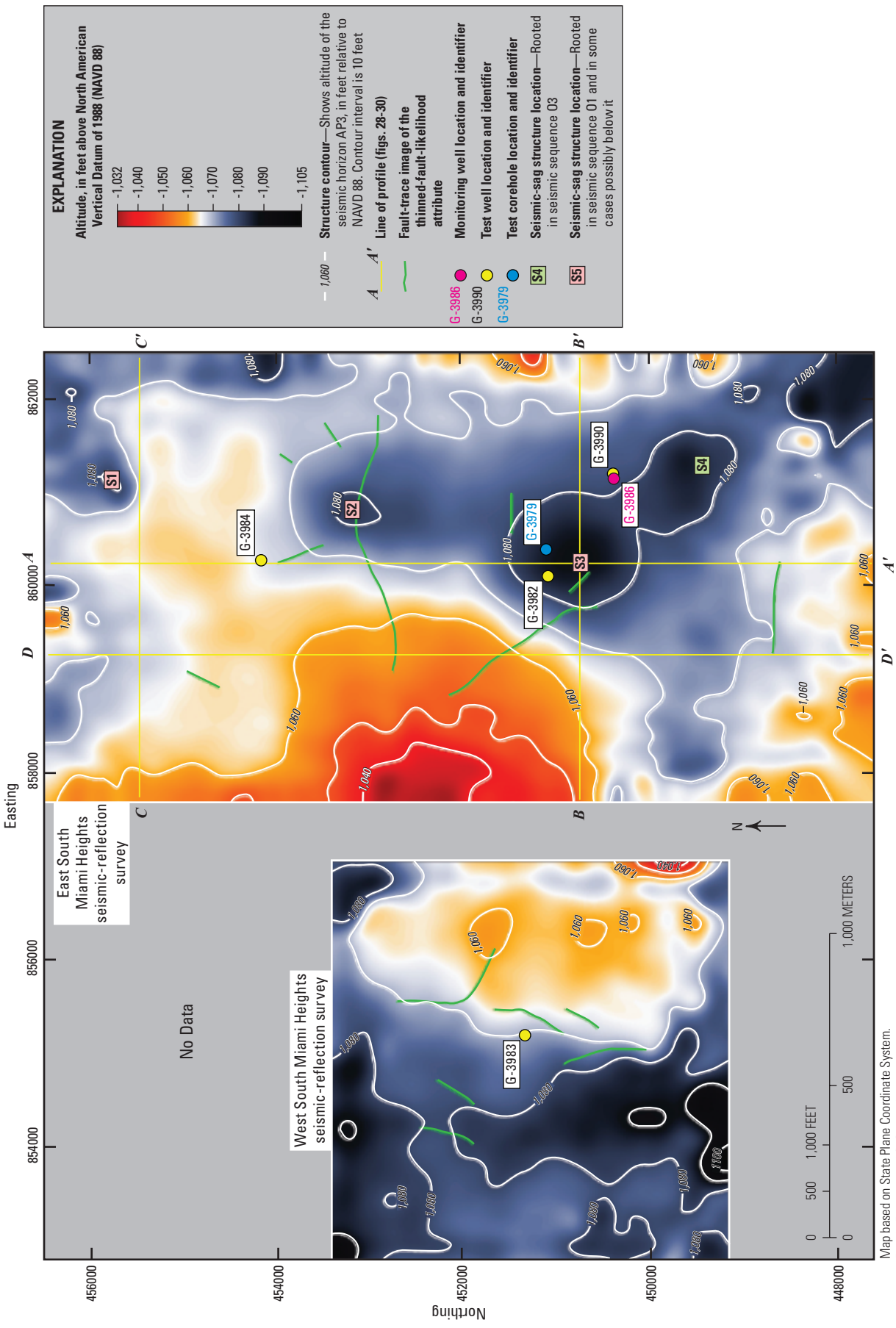

Figure 26. Structural altitude maps of the seismic horizon AP3 at the west and east South Miami Heights three-dimensional (3D) seismic survey areas (fig. 1).

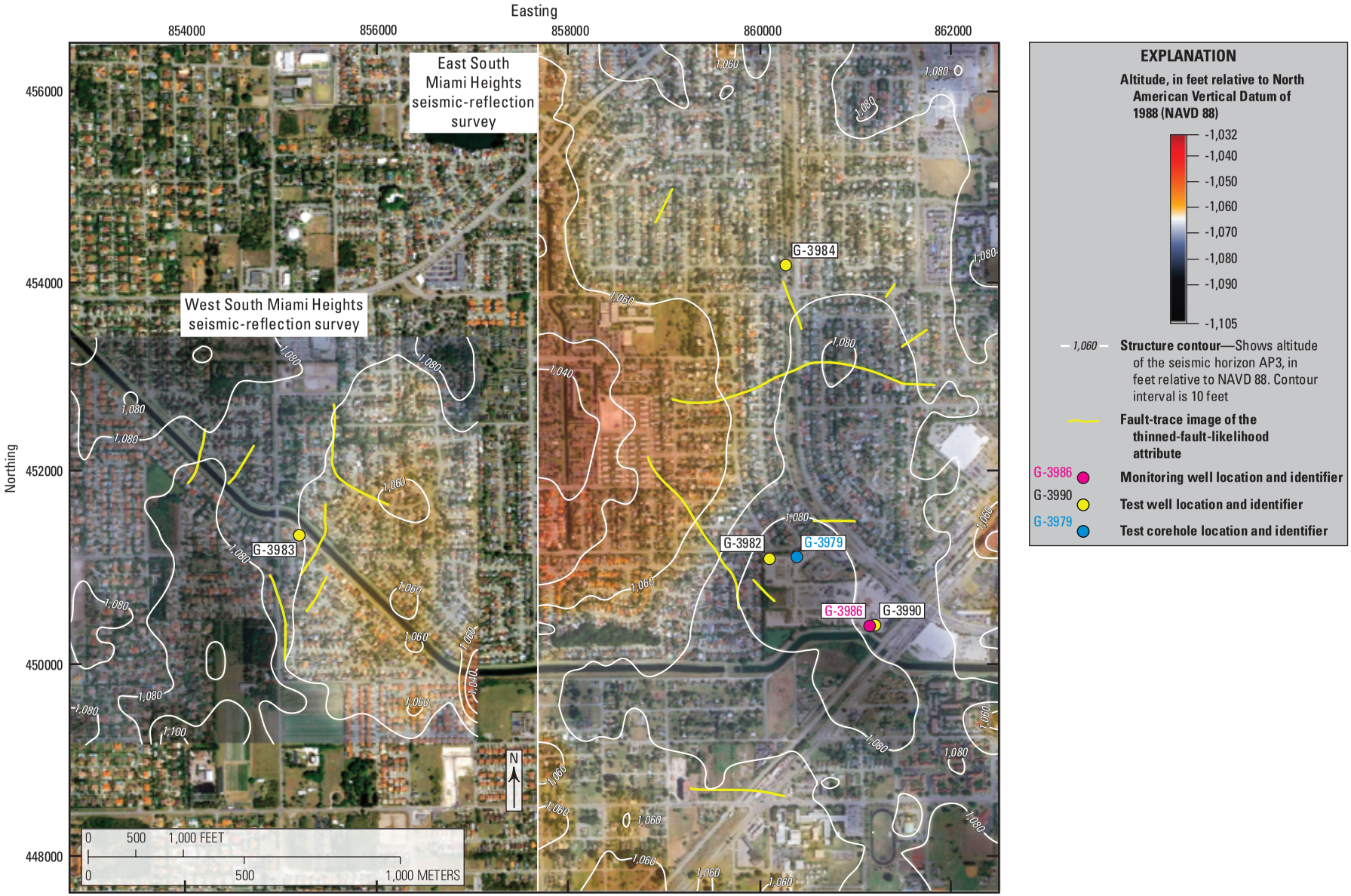

Base map data from Google, 2017.
Map based on State Plane Coordinate System.
Florida East 901 in U.S. Survey feet.
North American Datum of 1983

Figure 27. Structural altitude maps of seismic horizon AP3 at the west and east South Miami Heights three-dimensional (3D) seismic survey areas (fig. 1) overlain on an aerial image. The aerial imagery is included to show the relationship of the structural altitude map to the dense suburban development in the study area.

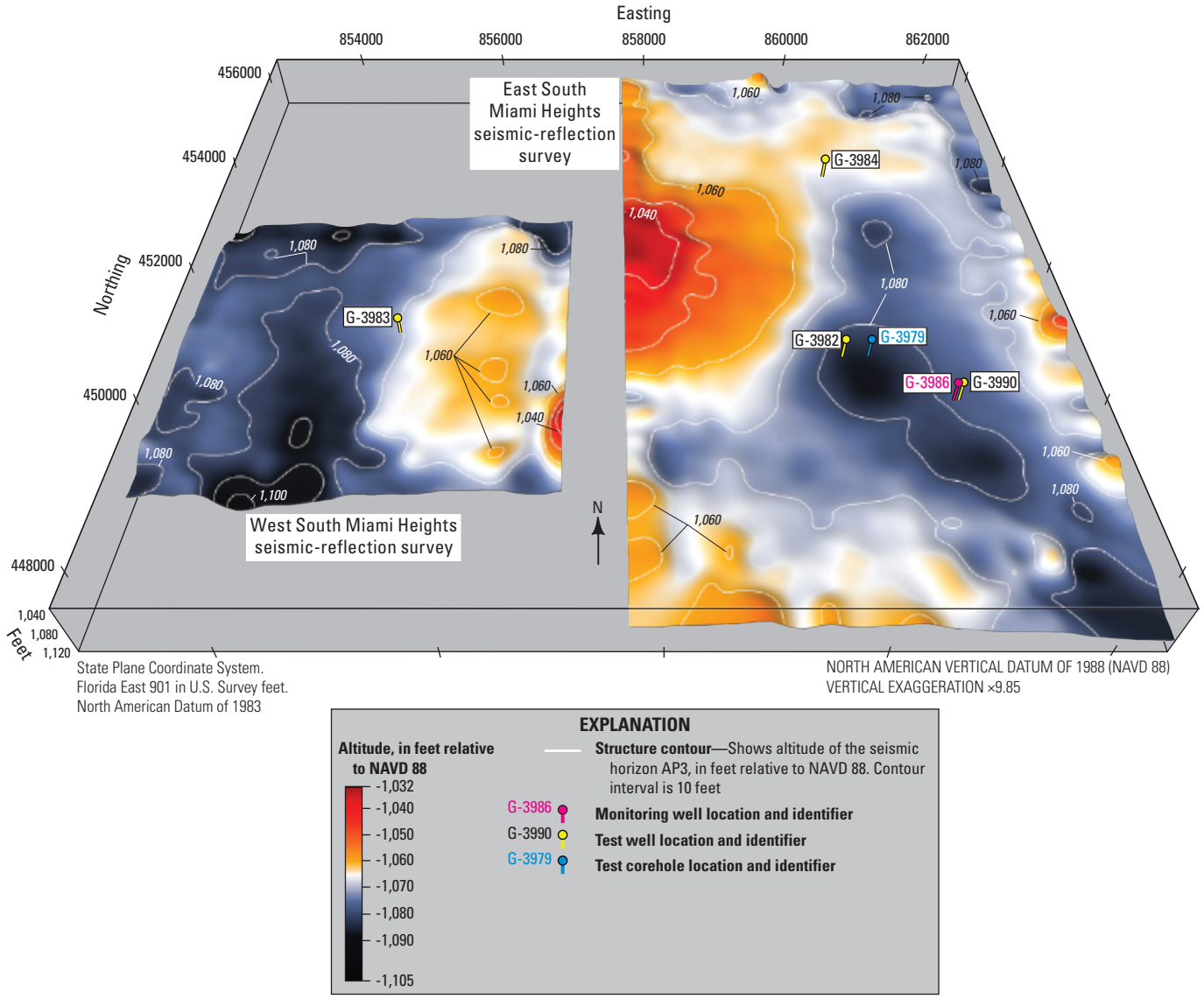

Figure 28. Oblique view, looking north, of three-dimensional (3D) structural altitude maps of seismic horizon AP3 in the west and east South Miami Heights survey 3D seismic survey areas (fig. 1).

two-way traveltime of about 485 ms and at about 70 ms acoustic two-way traveltime below the seismic horizon AP1. The lowermost vertical extent of the columniform seismic-sag structure is at an acoustic two-way traveltime of about 720 ms and at about 65 ms acoustic two-way traveltime below the seismic horizon O1, or perhaps deeper. Unlike columniform seismic-sag structure S3 in figure 13, seismic-sag structure S16 (fig. 25) is composed mostly of disturbed or chaotic seismic reflections on crossline 13 (fig. 25) and mostly disturbed sagging to chaotic reflections on inline 32 (fig. 25). Columniform seismic-sag structure S16 is interpreted as a zone of intense karstification that includes sagging strata, fractures, faults, and at least one instance of a "cave" (fig. 25). The total height of this columniform seismic-sag structure is about 1,200 ft, and the maximum width is about 1,900 ft at the level of seismic horizon O3. The uppermost termination of the S16 structure within rock in the lower part of the Avon Park Formation indicates the deformation of the structure occurred within in the mesogenetic zone during the middle Eocene (fig. 2) or later.

Seismic-Scale "Caves"

At South Miami Heights, bead-string reflections are considered indicators of seismic-scale "caves." The bead-string reflections in the study area typically are present along vertical faults (fig. 31), and in many instances, there is also an association with columniform seismic-sag structures (figs. 13, 14, 25). In some cases, they appear to be indicators of hypogenic karst (Zhu and others, 2017), especially where the bead strings shown are within or near sagging suprastratal reflections of columniform seismic-sag structures that formed in the mesogenetic burial zone (fig. 14). The bead-string reflections indicating "caves" in the lower to middle part of the

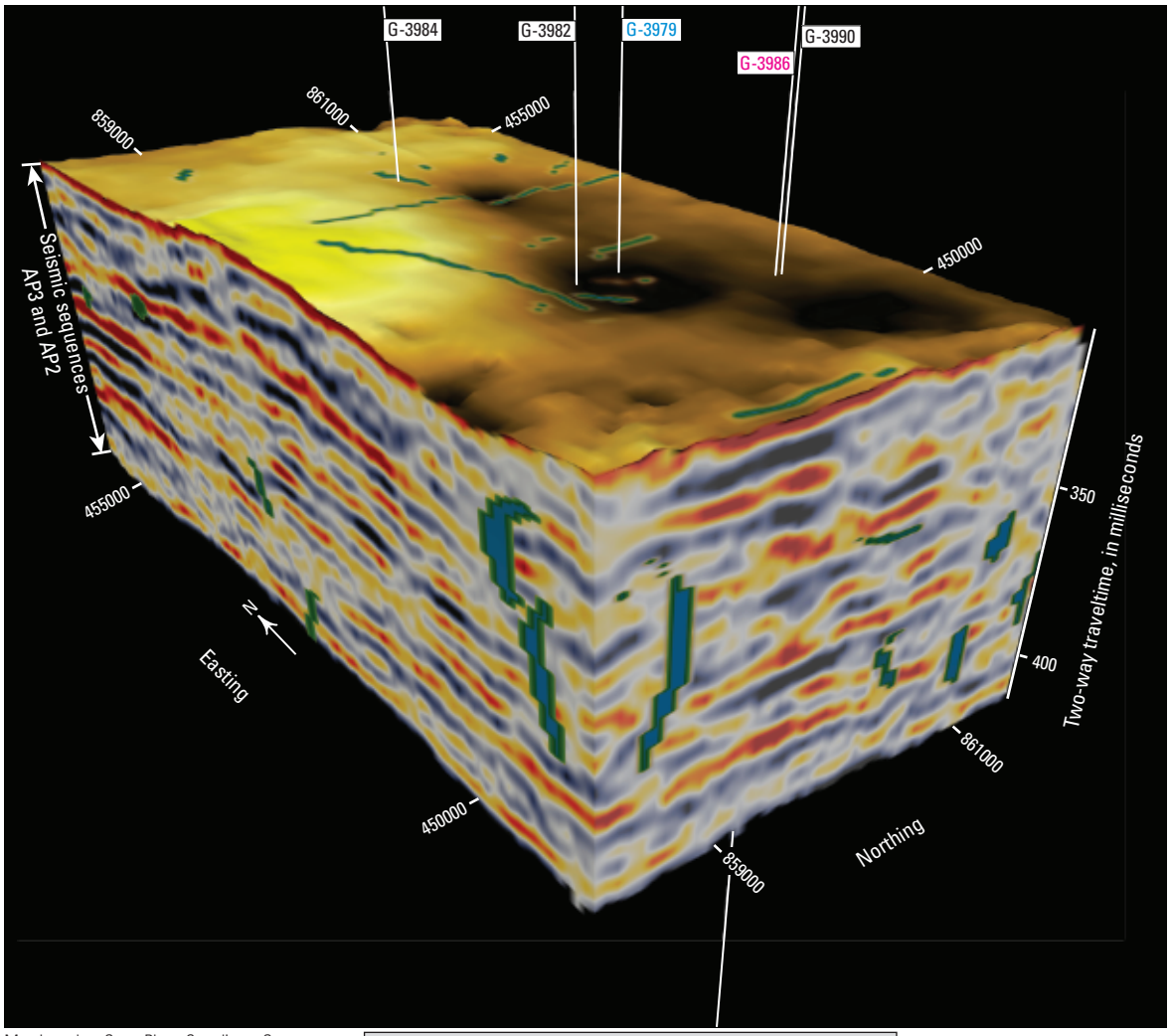

Figure 29. Seismic data volume of the east South Miami Heights three-dimensional (3D) seismic survey, including a time-structure map of the seismic horizon AP3 as the top surface and a time-structure map of seismic horizon AP1 as the base (fig. 2). The volume includes an entire thickness of seismic sequences AP2 and AP3 (fig. 2). The west side of the volume is a seismic profile along the inline direction, and the south side is a seismic profile along the crossline direction. Fault-trace images of the thinned-fault-likelihood attribute are shown along the sides and the upper seismic time-structure map.

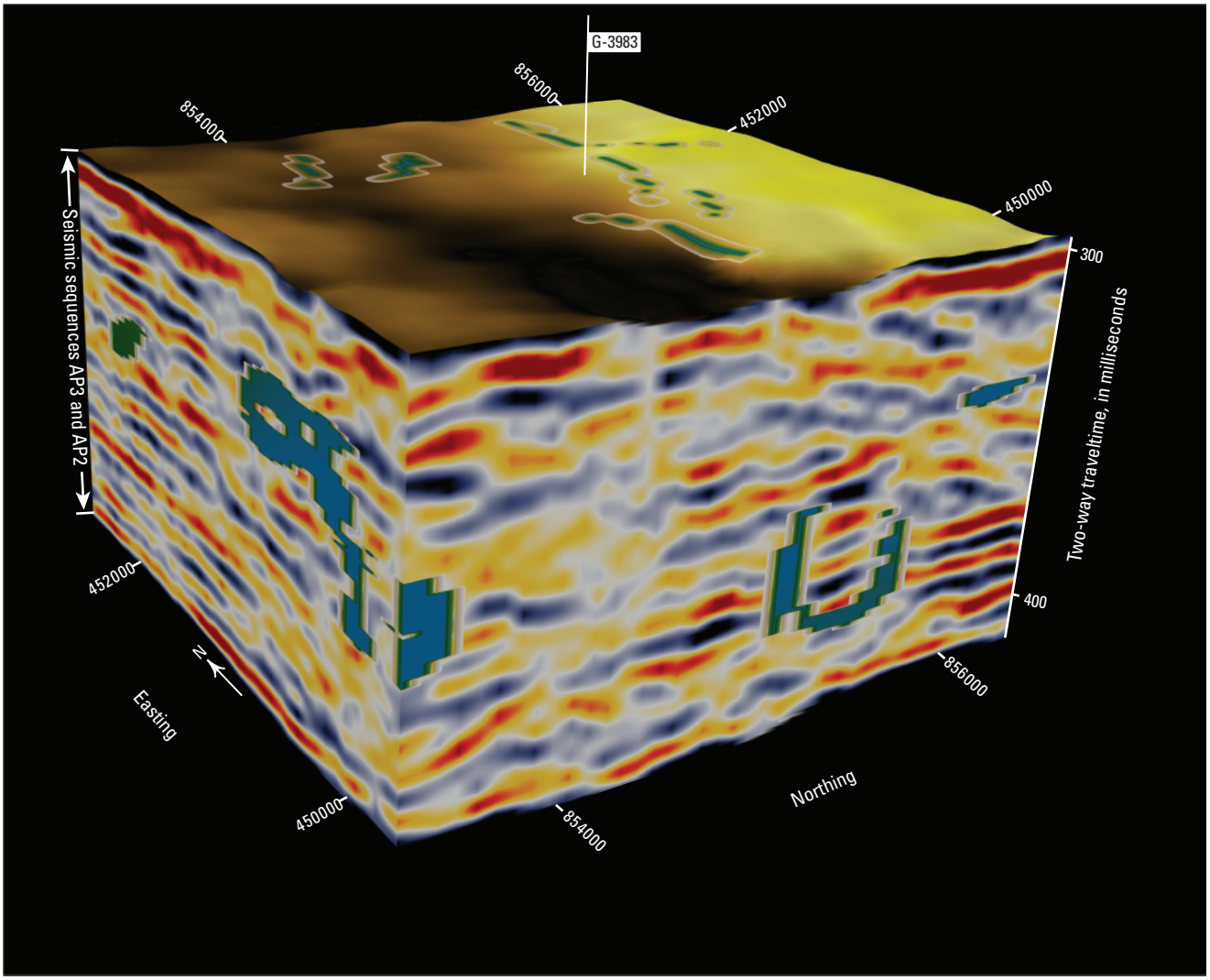

Map based on State Plane Coordinate System.
Florida East 901 in U.S. Survey feet.
North American Datum of 1983

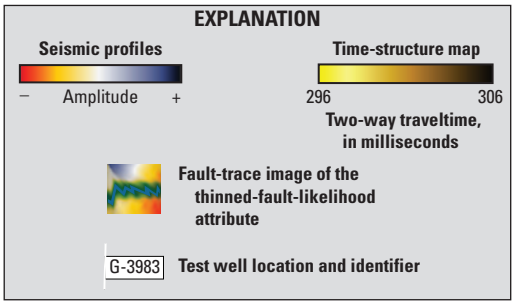

Figure 30. Seismic data volume of the west South Miami Heights three-dimensional (3D) seismic survey, including a time-structure map of the seismic horizon AP3 as the top surface and a time-structure map of seismic horizon AP1 as the base (fig. 2). The volume includes an entire thickness of seismic sequences AP2 and AP3 (fig. 2). The west side of the volume is a seismic profile along the inline direction, and the south side is a seismic profile along the crossline direction. Fault-trace images of the thinned-fault-likelihood attribute are shown along the sides and the upper seismic time-structure map.

Avon Park Formation (fig. 14) are suggested to have formed by movement of chemically aggressive water upward along faults after formation of the seismic sags; lateral transfer of the aggressive water into horizontal, permeable fluid-carrier beds cut by the faults; and lastly, formation of thick assemblages of fabric-selective vuggy megaporosity (Choquette and Pray, 1970 and "caves" by dissolution (Zhu and others, 2017). In the study area, the largest "cave" measured about 690 ft in width and about 210 ft in height, whereas the smallest "caves" measured about 190 ft in width and about 15 ft in height. These findings suggest that these minimum dimensions are the approximate lower limit needed for cave detection within the seismic data from the South Miami Heights study area.

Summary and Conclusions

Two three-dimensional seismic surveys over a surface area of 3.4 square miles were acquired in southeastern Miami-Dade County during June–August 2015 as part of an ongoing broad regional investigation by the U.S. Geological Survey and Miami-Dade Water and Sewer Department that includes mapping and karst characterization of the Floridan aquifer system in southeastern Florida. The seismic data were collected in a densely populated suburban setting using a vibroseis source and autonomous nodal receivers. This report presents 12 structural altitude maps of four seismic horizons, eight seismic data volumes that each include a time-structure map as the top surface, and four seismic profiles. The four seismic horizons are equivalent, or nearly equivalent, to the upper boundaries of seismic sequences and depositional sequences O1, O3, AP1, and AP3. In addition, the upper boundaries of the seismic sequences and depositional sequences O1, O3, AP1, and AP3 are equivalent, or nearly equivalent, to the tops of the Boulder Zone, uppermost major permeable zone of the Lower Floridan aquifer, Avon Park permeable zone, and Upper Floridan aquifer, respectively.

Computer-generated images of a thinned-fault-likelihood attribute are shown on eight of the structural altitude maps and all seismic data volumes. These fault-trace images indicate the likely presence for high-angle faults is greatest in the early Eocene shallow-marine carbonate (Oldsmar Formation) of the Lower Floridan aquifer, as compared to the overlying middle Eocene shallow-marine carbonate (Avon Park Formation) of the Floridan aquifer system. This difference reflects greater epigenic karstification during the early Eocene as compared to the middle Eocene, greater brittle deformation in the form of faulting and fracturing in the early Eocene rocks relative to middle Eocene rocks, and possibly greater tectonic

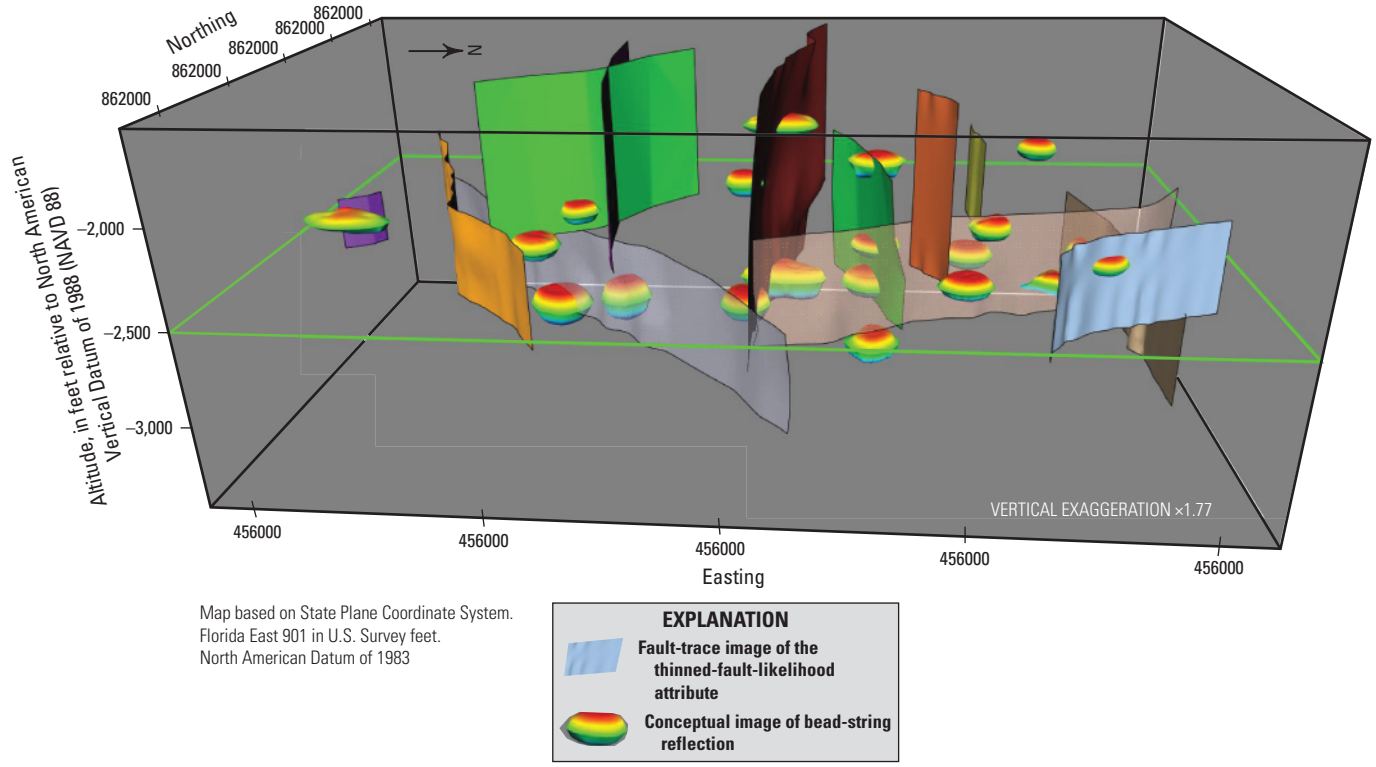

Figure 31. Block diagram showing three-dimensional (3D) ROXAR geomodel of seismic-scale "caves" identified in the east South Miami Heights seismic study area (fig. 1). The vertical extent of the model is from altitudes of 3,438 feet at the base to 1,560 feet at the top. Note the strong association of the "caves" and faults.

overprinting of the early Eocene rocks as compared to the middle Eocene rocks. The high-probability fault traces show where there is potential for high permeability fluid-flow passageways, probably with the highest concentration of flow where fault traces intersect. The mapping of these high-probability fault traces indicates a much higher probability of vertical cross-formational fluid flow along faults and fractures in the rocks of the Lower Floridan aquifer than in the overlying part of the Floridan aquifer system. The same relationship has also been reported for two-dimensional seismic profiles in eastern Broward County.

Twenty columniform seismic-sag structures were identified in the seismic data from the study area. The roots of fifteen of the columniform karst-collapse structures are mostly concentrated in the carbonate rock of the Oldsmar Formation, which is equivalent to the Boulder Zone, or in some cases deeper. The remaining five structures are rooted in the upper part of the Oldsmar Formation that is above the Boulder Zone. The upper termination of the twenty columniform karst-collapse structures ranges from the lower part of the Avon Park Formation (middle confining unit 2) to an upper part of the early to middle Miocene Arcadia Formation (middle part of the intermediate confining unit). The seismic-sag structures commonly consist of a lower and an upper seismic facies. The lower seismic facies is characterized by parallel sagging to chaotic reflection configurations and common anomalous bright spots called bead-string reflections, where the sagging to chaotic reflection configurations and bead-string reflections represent karst collapse and seismic-scale caves or paleocaves, respectively. Presumably, the lower seismic facies is a columnar volume of high permeability. The upper seismic facies is characterized entirely, or almost entirely, of continuous parallel reflection configurations that stack vertically and have a sagging reflection geometry. Seismic-scale caves, faults, and fractures are much less likely to be present in the upper seismic facies. The upper seismic facies is likely to have a lower permeability compared to the lower seismic facies. The lower seismic facies extends upward only into a lower part of the Avon Park Formation below the top of depositional sequence AP1 or the top of the Avon Park permeable zone. Thus, there may be relatively higher potential for the columniform karst-collapse structures to provide cross-formational fluid migration upward from the Boulder Zone into the lower part of the middle confining unit 2 as compared to a lower potential for cross-formational fluid migration from the upper part of the middle confining unit 2 further upward to the Upper Floridan aquifer.

The columniform karst-collapse structures are considered to have formed in the mesogenetic burial zone during the middle Eocene to middle Miocene or later. The structures formed by means of cave collapse or stoping or both, and consequent subsidence and sag of an overlying column of strata after burial. The extreme height of the columnar sagging overburden, as great as 2,700 ft, suggests a long-term interplay between collapse and hypogenic karstification within the columniform structures.

References

Baeten, G.J.M., 1989, Theoretical and practical aspects of the Vibroseis methods: Delft, Delft University of Technology, unpublished Ph.D. dissertation, 263 p.

Barnett, A.J., Wright, V.P., Chandra, V.S., and Jain, V., 2015, Distinguishing between eogenetic, unconformity-related and mesogenetic dissolution—A case study from the Panna and Mukta fields, offshore, Mumbai, India, *in* Armitage, P.J., Butcher, A.R., Churchill, J.M., Csoma, A.E., Hollis, C., Lander, R.H., Omma, J.E., and Worden, R.H., eds., Reservoir quality of clastic and carbonate rocks— Analysis, modelling and prediction: Geological Society, London, Special Publication 435, p. 67-84. [Also available at https://doi.org/10.1144/SP435.12.]

Bertoni, C., and Cartwright, J.A., 2005, 3D seismic analysis of circular evaporite dissolution structures, Eastern Mediterranean: London, Journal of the Geological Society, v. 162, p. 909–926. [Also available at http://jgs.lyellcollection.org/content/162/6/909.]

Betzler, C., Lindhorst, S., Hübscher, C., Lüdmann, T., Fürstenau, J., and Reijmer, J., 2011, Giant pockmarks in a carbonate platform (Maldives, Indian Ocean): Marine Geology, v. 289, no. 1-4, p. 1–16. [Also available at https://doi.org/10.1016/j.margeo.2011.09.004.]

Budd, D.A., Saller, A.H., and Harris, P.M., 1995, Unconformities and porosity in carbonate strata: American Association of Petroleum Geologists Memoir 63, 313 p. [Also available at http://archives.datapages.com/data/specpubs/memoir63/front/images/front.pdf.]

Burberry, C.M., Jackson, C.A.-L., and Chandler, S.R., 2016, Seismic reflection imaging of karst in the Persian Gulf—Implications for the characterization of carbonate reservoirs: American Association of Petroleum Geologists Bulletin, v. 100, no. 10, p. 1561–1584. [Also available at https://doi.org/10.1306/04151615115.]

Chapman, W.L., Brown, G.L., and Fair, D.W., 1981, The Vibroseis system—A high-frequency tool: Geophysics, v. 46, no. 12, p. 1657–1666. [Also available at https://doi.org/10.1190/1.1441173.]

Chen, D., Wu, S., Völker, D., Dong, D., Shi, H., Zhao, S., and Zhu, L., 2015, Tectonically induced, deep-burial paleo-collapses in the Zhujiang, Miocene carbonate platform in the northern South China Sea: Marine Geology, v. 364, p. 43–52. [Also available at https://doi.org/10.1016/j.margeo.2015.03.007.]

Choquette, P.W., and Pray, L.C., 1970, Geologic nomenclature and classification of porosity in sedimentary carbonates: American Association of Petroleum Geologists Bulletin, v. 54, no. 2, p. 207–250.

Cunningham, K.J., 2015, Seismic-sequence stratigraphy and geologic structure of the Floridan aquifer system near "Boulder Zone" deep wells in Miami-Dade County, Florida: U.S. Geological Survey Scientific Investigations Report 2015–5013, 28 p., accessed June 28, 2018, at https://doi.org/10.3133/sir20155013.

Cunningham, K.J., Bukry, D., Sato, T., Barron, J.A., Guertin, L.A., and Reese, R.S., 2001, Sequence stratigraphy of a south Florida carbonate ramp and bounding siliciclastics (Late Miocene-Pliocene): Florida Geological Survey Special Publication, v. 49, p. 35–66. [Also available at https://sofia.usgs.gov/publications/papers/fgssp49/fgsps49.cunningham.pdf.]

Cunningham, K.J., Locker, S.D., Hine, A.C., Bukry, D., Barron, J.A., and Guertin, L.A., 2003, Interplay of Late Cenozoic siliciclastic supply and carbonate response on the southeast Florida Platform: Journal of Sedimentary Research, v. 73, no. 1, p. 31–46. [Also available at https://doi.org/10.1306/062402730031.]

Cunningham, K.J., and Walker, C., 2009, Seismic-sag structural systems in Tertiary carbonate rocks beneath southeastern Florida, USA: Evidence for hypogenic speleogenesis?, *in* Klimchouk, A.B., and Ford, D.C., eds., Hypogene speleogenesis and karst hydrogeology of artesian basins: Simferopol, Ukraine, Ukrainian Institute of Speleology and Karstology, Special Paper no. 1, p. 151-158, accessed June 23, 2018, at http://institute.speleoukraine.net/libpdf/Cunningham%20Walker_SEISMIC-SAG%20STRUCTURAL%20SYSTEMS%20IN%20FLORIDA_HypoConf_2009.pdf.

Cunningham, K.J., Westcott, R.L., and Kluesner, J.W., Robinson, E., Walker, C., and Khan, S.A., 2018, Sequence stratigraphy, seismic stratigraphy, and seismic structures of the lower intermediate confining unit and most of the Floridan aquifer system, Broward County, Florida (ver. 1.1, January 2018): U.S. Geological Survey Scientific Investigations Report 2017-5109, 71 p., 21 pls. [Also available at https://pubs.er.usgs.gov/publication/sir20175109.]

Dausman, A.M., Doherty, J., Langevin, C.D., and Dixon, J., 2010, Hypothesis testing of buoyant plume migration using a highly parameterized variable-density groundwater model at a site in Florida, USA: Hydrogeology Journal, v. 18, no. 1, p. 147–160. [Also available at https://doi.org/10.1007/s10040-009-0511-6.]

Ebuna, D.R., Kluesner, J.W., Cunningham, K.J., and Edwards, J.H., 2018, Statistical approach to neural network imaging of karst systems in 3D seismic reflection data: Interpretation, v. 6, no. 3, p. B15-B35. [Also available at http://dx.doi.org/10.1190/INT-2017-0197.1.]

Field, M.S., 2002, A lexicon of cave and karst terminology with special reference to environmental karst hydrology: U.S. Environmental Protection Agency Technical Report EPA/600/R-02/003, 214 p. [Also available at https://cfpub.epa.gov/ncea/risk/recordisplay.cfm?deid=54964.]

Fish, J.E., and Stewart, M., 1991, Hydrogeology of the surficial aquifer system, Dade County, Florida: U.S. Geological Survey Water-Resources Investigations Report 90-4108, 50 p. [Also available at https://pubs.er.usgs.gov/publication/wri904108.]

Guertin, L.A., Missimer, T.M., and McNeill, D.F., 2000, Hiatal duration of correlative sequence boundaries from Oligocene—Pliocene mixed carbonate/siliciclastic sediments of the south Florida Platform: Sedimentary Geology, v. 134, no. 1-2, p. 1–26. [Also available at https://doi.org/10.1016/S0037-0738(00)00011-7.]

Hardage, B.A., Carr, D.L., Lancaster, D.E., Simmons, J.L., Jr., Elphick, R.Y., Pendleton, V.M., and Johns, R.A., 1996, 3-D seismic evidence of the effects of carbonate karst collapse on overlying clastic stratigraphy and reservoir compartmentalization: Geophysics, v. 61, no. 5, p. 1336–1350. [Also available at https://doi.org/10.1190/1.1444057.]

Hess, J.W., 2005, Pits and shafts, *in* Culver, D.C., and White, W.B., eds., Encyclopedia of caves: Burlington, MA, Elsevier Academic Press, p. 444-447.

Heubeck, C., Story, K., Peng, P., Sullivan, C., and Duff, S., 2004, An integrated reservoir study of the Liuhua 11–1 field using a high-resolution three-dimensional seismic data set, *in* Eberli, G.P., Masaferro, J.L., and Sarg, J.F., eds., Seismic imaging of carbonate reservoirs and systems: American Association of Petroleum Geologists Memoir, v. 81, p. 149–168.

Hine, A.C., Suthard, B.C., Locker, S.D., Cunningham, K.J., Duncan, D.S., Evans, M., and Morton, R.A., 2009, Karst sub-basins and their relationship to the transport of Tertiary siliciclastic sediments on the Florida Platform: International Association of Sedimentologists Special Publication 41, p. 179–197. [Also available at https://onlinelibrary.wiley.com/doi/abs/10.1002/9781444312065.ch12.]

Kindinger, J.L., Davis, J.B., and Flocks, J.G., 1999, Geology and evolution of lakes in north-central Florida: Environmental Geology, v. 38, no. 4, p. 301–321, accessed June 23, 2018, at https://doi.org/10.1007/s002540050428.

Klimchouk, A., and Ford, D., 2000, Types of karst and evolution of hydrogeologic setting, *in* Klimchouk, A.B., Ford, D.C., Palmer, A.N., and Dreybrodt, Wolfgang, eds., Speleogenesis—evolution of karst aquifers: Huntsville, Ala., National Speleological Society Inc., 45-53 p.

Loucks, R.G., 1999, Paleocave carbonate reservoirs—Origins, burial-depth modifications, spatial complexity, and reservoir management: American Association of Petroleum Geologists, v. 83, p. 1795–1834.

Liu, Y., and Wang, Y., 2017, Seismic characterization of a carbonate reservoir in Tarim Basin: Geophysics, v. 82, no. 5, p. B177–B188. [Also available at https://doi.org/10.1190/geo2016-0517.1.]

Maliva, R.G., Guo, W., and Missimer, T., 2007, Vertical migration of municipal wastewater in deep injection well systems, South Florida, USA: Hydrogeology Journal, v. 15, no. 7, p. 1387–1396. [Also available at https://doi.org/10.1007/s10040-007-0183-z.]

McDonnell, A., Loucks, R.G., and Dooley, T., 2007, Quantifying the origin and geometry of circular sag structures in northern Fort Worth Basin, Texas—Paleocave collapse, pull-apart fault systems, or hydrothermal alteration?: The American Association of Petroleum Geologists Bulletin, v. 91, no. 9, p. 1295–1318. [Also available at https://doi.org/10.1306/05170706086.]

Meyer, F.W., 1974, Evaluation of hydraulic characteristics of a deep artesian aquifer from natural water-level fluctuations, Miami, Florida: Florida Bureau of Geology Report of Investigations 75, 32 p. [Also available at https://pubs.er.usgs.gov/publication/70046940.]

Meyer, F.W., 1989, Hydrogeology, ground-water movement, and subsurface storage in the Floridan aquifer system in southern Florida: U.S. Geological Survey Professional Paper 1403-G, 59 p. [Also available at https://pubs.usgs.gov/pp/1403g/report.pdf.]

Miller, J.A., 1986, Hydrogeologic framework of the Floridan aquifer system in Florida and in parts of Georgia, Alabama, and South Carolina: U.S. Geological Survey Professional Paper 1403-B, 91 p. [Also available at https://pubs.er.usgs.gov/publication/pp1403B.]

Mitchum, R.M., Jr., Vail, P.R., and Sangree, J.B., 1977, Seismic stratigraphy and global changes of sea level, Part 6—Stratigraphic interpretation of seismic reflection patterns in depositional sequences, *in* Payton, C.E., ed., Seismic stratigraphy—Applications to hydrocarbon exploration: American Association of Petroleum Geologists Memoir 26, p. 117–133.

Monroe, W.H., (compiler), 1972, A glossary of karst terminology (2d ed): U.S. Geological Survey Water-Supply Paper 1899-K, 26 p., accessed June 28, 2018, at https://pubs.usgs.gov/wsp/1899k/report.pdf.

Morettini, E., Thompson, A., Eberli, G.P., Rawnsley, K.D., Asyee, W., Christman, P., Cortis, T., Foster, K., Hitchings, V., Kolkman, W., and Van Konijnenburg, J.H., 2005, Combining high resolution sequence stratigraphy and mechanical stratigraphy for improved reservoir characterisation in the Fahud field of Oman: GeoArabia, v. 10, p. 17–44.

Popenoe, P., Kohout, F.A., and Manheim, F.T., 1984, Seismic-reflection studies of sinkholes and limestone dissolution features on the northeastern Florida shelf, *in* Beck, B.F., ed., Sinkholes—Their geology, engineering, and environmental impact: Proceedings of First Multidisciplinary Conference on Sinkholes, p. 43–57.

Rao, Y., and Wang, Y., 2015, Seismic signatures of carbonate caves affected by near-surface absorptions: Journal of Geophysics and Engineering, v. 12, no. 6, p. 1015–1023. [Also available at https://doi.org/10.1088/1742-2132/12/6/1015.]

Spechler, R.M., 2001, The relation between structure and saltwater intrusion in the Florida aquifer system, northeastern Florida, *in* Kuniansky, E.L., ed., U.S. Geological Survey Karst Interest Group Proceedings, Water-Resources Investigations Report 01-4011 p. 25–29. [Also available at https://water.usgs.gov/ogw/karst/kigconference/rms_relationintrusion.htm.]

Sun, Q., Cartwright, J., Wu, S., and Chen, D., 2013, 3D seismic interpretation of dissolution pipes in the South China Sea: Genesis by subsurface, fluid induced collapse: Marine Geology, v. 337, p. 171-181. [Also available at https://doi.org/10.1016/j.margeo.2013.03.002.]

U.S. Environmental Protection Agency, 2013, Underground injection control glossary: U.S. Environmental Protection Control Web page, accessed June 28, 2018, at https://ofmpub.epa.gov/sor_internet/registry/termreg/searchandretrieve/glossariesandkeywordlists/search.do?details=&glossaryName=UIC%20Glossary.

Walsh, V., and Price, R.M., 2010 Determination of vertical and horizontal pathways of injected fresh wastewater into a deep saline aquifer (Florida, USA) using natural chemical tracers: Hydrogeology Journal, v. 18, 1027-1042. [Also available at https://doi.org/10.1007/s10040-009-0570-8.]

Waltham, T., 2002, The engineering classification of karst with respect to the role and influence of caves: International Journal of Speleology, v. 31, p. 19-35. [Also available at http://scholarcommons.usf.edu/cgi/viewcontent.cgi?article=1230&context=ijs.]

Xu, C., Di, B., and Wei, J., 2016, A physical modeling study of seismic features of karst cave reservoirs in the Tarim Basin, China: Geophysics, v. 81, no. 1, p. B31-B41. [Also available at https://doi.org/10.1190/geo2014-0548.1.]

Zeng, H., Wang, G., Janson, X., Loucks, R., Xia, Y., Xu, L., and Yuan, B., 2011a, Characterizing seismic bright spots in deeply buried, Ordovician paleokarst strata, Central Tabei uplift, Tarim Basin, Western China: Geophysics, v. 76, no. 4, p. B127–B137. [Also available at https://doi.org/10.1190/1.3581199.]

Zeng, H., Loucks, R., Janson, X., Wang, G., Xia, Y., Yuan, B., and Xu, L., 2011b, Three-dimensional seismic geomorphology and analysis of the Ordovician paleokarst drainage system in the central Tabei Uplift, northern Tarim Basin, western China: The American Association of Petroleum Geologists Bulletin, v. 95, no. 12, p. 2061–2083. [Also available at https://doi.org/10.1306/03111110136.]

Zhiqian, G., and Tailiang, F., 2015, Unconformities and their influence on lower Paleozoic petroleum reservoir development in the Tarim Basin: Journal of Petroleum Science Engineering, v. 133, p. 335–351. [Also available at https://doi.org/10.1016/j.petrol.2015.06.015.]

Zhu, H., Zhu, X., and Chen, H., 2017, Seismic characterization of hypogenic karst systems associated with deep hydrothermal fluids in the Middle-Lower Ordovician Yingshan Formation of the Shunnan area, Tarim Basin, NW China: Geofluids, v. 2017, 13 p. [Also available at https://doi.org/10.1155/2017/8094125.]

Zuo, J.-P., Peng, S.-P., Li, Y.-J., Chen, Z.-H., and Xie, H.-P., 2009, Investigation of karst collapse based on 3-D seismic technique and DDA methods at Xieqiao coal mine, China: International Journal of Coal Geology, v. 78, no. 4, p. 276–287. [Also available at https://doi.org/10.1016/j.coal.2009.02.003.]

For more information about this publication, contact

Director, Caribbean-Florida Water Science Center
U.S. Geological Survey
4446 Pet Lane, Suite 108
Lutz, FL 33559
(813) 498-5000

For additional information visit
https://www2.usgs.gov/water/caribbeanflorida/index.html

Publishing support provided by
Lafayette Publishing Service Center

ISSN 2328-0328 (online)
https://doi.org/10.3133/sir20185117